Complex roles of the actin-binding protein Girdin/GIV in DNA damage-induced apoptosis of cancer cells

Chen Chen[1], Atsushi Enomoto[1]*, Liang Weng[3,4], Tetsuro Taki[1], Yukihiro Shiraki[1], Shinji, Mii[1], Ryosuke Ichihara[1], Mitsuro Kanda[2], Masahiko Koike[2], Yasuhiro Kodera[2] & Masahide Takahashi[1,5]*

[1]Department of Pathology, [2]Department of Gastroenterological Surgery (Surgery II), Nagoya University Graduate School of Medicine, Nagoya, 466-8550, Japan

[3]Center for Molecular Medicine, Xiangya Hospital, Central South University, 87 Xiangya Road, 410008, Changsha, Hunan, China

[4]Key Laboratory of Molecular Radiation Oncology Hunan Province, 410008, Changsha, Hunan, China

[5]International Center for Cell and Gene Therapy, Fujita Health University, Toyoake, 470-1192, Japan

Running title: The role of Girdin in DNA damage-induced apoptosis

Address correspondence to: Atsushi Enomoto (enomoto@iar.nagoya-u.ac.jp) and Masahide Takahashi (mtakaha@med.nagoya-u.ac.jp), Department of Pathology, Nagoya University Graduate School of Medicine, Nagoya, 466-8550, Japan. Tel: +81-52-744-2093. Fax: +81-52-744-2098.

Word count: 5010 words

Number of tables: 1

Number of figures: 6

Quantity of supporting information: 1 Supporting Methods and 6 Supporting figures

Abstract

The actin-binding protein Girdin is a hub protein that interacts with multiple proteins to regulate motility and Akt and trimeric G protein signaling in cancer cells. Girdin expression correlates with poor outcomes in multiple human cancers. However, those findings are not universal, as they depend on study conditions. Those data suggest that multiple aspects of Girdin function and its role in tumor cell responses to anticancer therapeutics must be reconsidered. In the present study, we found that Girdin is involved in DNA damage-induced cancer cell apoptosis. An esophageal cancer cell line that exhibited high Girdin expression showed a marked sensitivity to ultraviolet (UV)-mediated DNA damage compared to a line with low Girdin expression. When transcriptional activation of endogenous Girdin was mediated by an engineered CRISPR/Cas9 activation system, sensitivity to DNA damage increased in both stationary and migrating HeLa cancer cells. High Girdin expression was associated with dysregulated cell cycle progression and prolonged G1 and M phases. These features were accompanied by p53 activation, which conceivably increases cancer cell vulnerability to UV exposure. These data highlight the importance of understanding complex Girdin functions that influence cancer cell sensitivity to therapeutics.

Abbreviations: UVC, ultraviolet C

Keywords: DNA damage, apoptosis, Girdin, cell cycle, cancer cell heterogeneity, cell migration

1. Introduction

Cancer cells develop remarkable mechanisms to promote their uncontrolled proliferation, survival and motility. These characteristics contribute to their invasion of neighboring tissues and metastasis to distant organs (1). Treating cancers by various therapeutic modalities such as radiation and chemotherapeutic reagents is often unsatisfactory because the tumor cells gain therapeutic resistance leading to subsequent recurrence (1-4). The mechanisms of cancer therapeutic resistance have been the subject of intensive studies. Obviously, one of the most important causes of the therapeutic resistance is genetic and non-genetic heterogeneity and alterations of cancer cells, which becomes more prominent and elaborate by cancer cell evolution during the progression of the diseases and treatments (5, 6). The presence of cancer stem cells and dormant cancer cells is another cause of therapeutic resistance in multiple cancers (7, 8).

Girdin, which is also known as Gα-interacting vesicle-associated protein (GIV), was previously identified as an actin-binding protein and a substrate of Akt that is involved in the remodeling of the actin cytoskeleton (9, 10). It is essential for actin remodeling at the leading edge of migrating cancer cells (9). Girdin is crucial for cell migration as well as cell polarization and membrane trafficking (9, 11, 12). It also participates in Akt and heterotrimeric G protein signaling downstream of growth factors and cytokines through interactions with numerous proteins (9, 10, 13). Girdin-deficient mice exhibit a severe defect in collective migration of newborn neurons in postnatal and adult brains (14). These findings gave rise to the idea that Girdin is a conserved regulator of collective behavior of cells across many cell types (15). Indeed, we recently reported that Girdin plays an essential role in the collective invasion of human cancer cells (16). Supporting this view, many

studies have shown that high Girdin expression correlates with poor outcomes of patients with cancers of the breast, colon and esophagus (17-21).

Other seminal studies have shown that Girdin functions as a hub protein that controls the migration-proliferation dichotomy ("Go or Grow" mechanism) in HeLa cancer cells (22). Cyclin-dependent kinase 5 (Cdk5)-mediated phosphorylation of Girdin has a crucial role in promoting cell migration, whereas the non-phosphorylated form of Girdin promotes cell proliferation (23). Given the general view that migratory cells are essentially not proliferative and are resistant to DNA damage and cytotoxic reagents (24, 25), the migration-proliferation dichotomy has a central role in tumor cells' resistance to anticancer therapeutics. Nonetheless, cell proliferation capacity is undoubtedly essential for cancer progression, rendering the role of high Girdin expression in cancer progression rather unclear.

Another issue in evaluating the significance of Girdin expression in cancer progression is that its expression is not limited to tumor cells. That is, it is also found in endothelial cells and cancer-associated fibroblasts (CAFs) that constitute the tumor microenvironment, which confounds the interpretation of data obtained from mRNA extracted from whole tumors (26, 27). Indeed, in contrast to previous studies that showed a correlation of high Girdin expression in breast cancer cells to the poor outcome of the patients (28), our previous study showed that Girdin activation in CAFs did not correlate with patient outcomes (27). Interestingly, another study showed that Girdin is also expressed by brain tumor stem cells (BTSCs) derived from human glioblastomas and is involved in the maintenance of BTSC stemness (29). Girdin interacts with the 4F2 heavy chain, a subunit of multiple amino acid transporters, to negatively regulates amino acid signaling involving the mechanistic target of rapamycin complex 1 (mTORC1), further

showing the complexity of Girdin function (30). Consistent with these findings, a recent study showed that mTORC1 signaling is suppressed in BTSCs rather than activated as non-tumor stem cells in human gliomas (31), implying that Girdin may contribute to the resistance of BTSCs to existing therapeutics by suppressing their metabolism.

In the present study, we examined the effect of Girdin expression on cancer cells' sensitivity to cytotoxic therapeutics. We selected ultraviolet C (UVC)-induced DNA damage as a model of radiation therapy. We first found that high Girdin expression was associated with an increased sensitivity of cancer cells to UVC-mediated DNA damage. Interestingly, migratory cells, which are known to exhibit significant resistance to DNA damage-induced apoptosis, became prone to that by Girdin overexpression. This result suggested that high Girdin expression counteracts or eliminates the DNA damage protective effect of Girdin-mediated cell migration. Finally, we attempted to address the mechanism of this observation by identifying a novel role of Girdin in cell cycle regulation. These data suggested the presence of complex positive and negative roles of Girdin in cancer progression that depended on the cancer type and therapeutic context. These finding should be considered in the development of therapeutics that target pathways involving Girdin.

2. Materials and Methods

2.1 Human tissue samples

Biopsy and surgically resected esophageal tissue samples from 28 esophageal squamous cell carcinoma patients, who had provided informed consent, were obtained at Nagoya University Hospital from 2006 to 2017 (Table 1). This study was conducted in accordance with the Helsinki Declaration for Human Research and approved by the Ethics Committee of Nagoya University Graduate School of Medicine (approval number: 2017-0127).

2.2 Antibodies and Reagents

The following antibodies were used in this study: anti-Girdin (R&D Systems, Minneapolis, MN), anti-Girdin (IBL, Gunma, Japan), anti-Girdin phospho S1647 (ECM Biosciences), anti-histone H3 (1B1B2) (Cell Signaling Technology), anti-histone H3 phospho S10 (Abcam, Cambridge, UK), anti-histone H3 phospho S28 (Abcam), anti-cleaved PARP1 (Abcam), anti-Cleaved PARP1 (Cell Signaling Technology), anti-Rb phospho Ser795 (New England BioLabs, Ipswich, MA), anti-Rb (4H1) (Cell Signaling Technology), anti-p53 (Cell Signaling Technology), anti-p53 phospho S15 (Cell Signaling Technology), anti-p53 phospho S46 (Cell Signaling Technology), anti-Mad2 (C-10) (Santa Cruz Biotechnology), anti-α-Tubulin (Sigma-Aldrich), anti-γ-Tubulin (Sigma-Aldrich), Alexa Fluor 488 goat anti-mouse IgG (Thermo Fisher Scientific, Pittsburgh, PA), Alexa Fluor 488 goat anti-rabbit IgG (Thermo Fisher Scientific), rabbit anti-sheep IgG (H+L), Human SP ads-HRP (Southern Biotech, Birmingham, AL), and rabbit anti-rat IgG H&L (HRP) (Abcam) antibodies.

2.3 Cell lines and cell culture

KYSE140 and KYSE150 cell lines (32) were purchased from the JCRB Cell Bank (Osaka, Japan) and cultured in Ham's F-12 Nutrient Mix, GlutaMAX medium (Gibco 31765035, Thermo Fisher Scientific, Waltham, MA) supplemented with 5% fetal bovine serum (FBS) (Gibco 10270-106). The HeLa cell line was purchased from the American Type Culture Collection (Rockville, MD). HEK293T cells were purchased from Invitrogen (Carlsbad, CA). HeLa cells and HEK293T cells were cultured in Dulbecco's Modified Eagle Medium (#08458-16, Nacalai Tesque, Kyoto, Japan) supplemented with 10% FBS. Cells were cultured at 37°C in 5% CO_2 humidified air. The authenticity of HeLa cells (STR profile analysis) was verified by BEX Co., Ltd. (Tokyo, Japan). Cell lines were routinely tested for mycoplasma contamination by staining with DAPI (4', 6-diamidino-2-phenylindole) every 3 months.

2.4 Induction of DNA damage by UVC radiation

The culture medium was aspirated, and the cells were exposed at a dose of 20 or 100 J/m^2 of UVC radiation with Microprocessor-Controlled UV Crosslinkers (Spectroline, Westbury, NY) or were mock treated. Following the exposure, fresh medium was added, and the cells were incubated at 37°C with 5% CO_2 for indicated periods of time.

2.5 Establishment of a cell line that stably overexpresses Girdin

A HeLa cell line that stably overexpresses Girdin via the endogenous *CCDC88A* promoter was established by the CRISPR/single-guide RNA (sgRNA)-directed synergistic activation mediator (SAM) system (33). The sgRNA was designed using the CRISPR design website

(http://sam.genome-engineering.org/database_request/) and the guide sequence (5'-TTTCTTCTCCCACAATCCAG-3') was selected and cloned into the lenti-sgRNA (MS2)-pure vector (#73795, Addgene, Watertown, MA) using the Golden-Gate sgRNA cloning protocol described on http://sam.genome-engineering.org/protocols/. Sequencing for the constructed plasmid was done before use. Lentiviruses expressing dCas9-VP64 and MS2-P65-HSF1 were generated by transfection of the packaging plasmids psPAX2 (#12260, Addgene), pMD2.G (#12259, Addgene), and lenti dCAS-VP64_Blast (#61425, Addgene) or lenti MS2-P65-HSF1_Hygro (#61426, Addgene) into HEK293T cells using Lipofectamine 2000 (Thermo Fisher Scientific). HeLa cells were infected with the viruses, followed by selection in the presence of blasticidin (Wako, Osaka, Japan) and hygromycin (Invitrogen, Carlsbad, CA). Afterwards, the cells expressing the SAM components were transduced with lentiviruses expressing the *CCDC88A* sgRNA. After 48 h of infection, the cells were selected with puromycin (Sigma-Aldrich) for 14 days, replacing the puromycin every 3 days. All of the experiments using lentivirus vectors were performed in a BSL2 environment approved by Nagoya University.

2.6 Cell synchronization

Cells were treated with 60 ng/mL of nocodazole (Sigma-Aldrich) for 16 h. The mitotic cells were collected by mechanical shake-off (34), washed with PBS, and seeded on plates. The cells were harvested at different time points for cell cycle analysis. For cell synchronization at the G1/S boundary, cells were treated with 2 mM thymidine for 15 h, washed with PBS, grown for 10 h in a regular medium, and then treated again with 2 mM thymidine for 15 h,

followed by wash with PBS. This marks time 0, after which the cells were collected at the indicated times for analysis.

2.7 Flow cytometric analysis

For the quantitation of mitotic cells, cells were probed with anti-histone H3 (phospho S10) antibody (Abcam). Cells were collected and incubated with anti-histone H3 (phospho S10) antibody for 1 h at room temperature in the dark. Cells were fixed with 4% paraformaldehyde for 15 min, followed by resuspension in solution with Alexa Fluor 488-conjugated rabbit anti-mouse IgG (Thermo Fisher Scientific) for 30 min at room temperature in the dark. Data acquisition was performed using FACS Canto2 (BD Biosciences, San Jose, CA) and results were analyzed with FlowJo software (BD Biosciences).

To quantitate the DNA content by flow cytometry, the propidium iodide (PI) flow cytometry kit (Abcam) was used according to the manufacturer's instruction. Cells were collected and fixed by the addition of 66% ethanol at 4°C. On the following day, cells were treated with propidium iodide and RNase at 37°C for 30 min. The modeling of DNA content histograms was done by using ModFitLT software (Verity Software House).

2.8 Statistical analysis

Significant differences were determined by two-tailed *t*-tests for comparison of the means between two sets of data, or one-way ANOVA for comparison of the means among 3 or

more sets of data using GraphPad Prism (GraphPad Software, San Diego, CA). All graphs represent mean ± standard deviation (SD). $P < 0.05$ was regarded as significant. For the analysis of overall survival of the patients, data were plotted using Kaplan-Meier analysis in GraphPad Prism and the significant differences were evaluated with a log-rank test.

2.9 Data availability

The data that support the findings of this study are available from the corresponding author upon reasonable request.

3. Results

3.1 Prognostic values of Girdin expression levels in esophageal cancer: variations and inconsistencies

Previous studies showed a significant correlation between Girdin (*CCDC88A*) mRNA expression levels and poor clinical outcomes in esophageal cancer (17). Those data were consistent with other studies showing correlations of Girdin expression with poor outcomes of many types of cancer (18 – 21, 28). Our analysis of esophageal cancer cases in the TCGA dataset, however, resulted in variable Kaplan-Meier survival curves and log-rank P-values that fluctuated depending on cut-off values (**Fig. 1A-C**). Girdin gene expression levels correlated with favorable prognosis of the patients with an empirically determined

cut-off value (75%). However, with other values (25 and 50%), they showed no correlation with the prognosis.

We used immunohistochemistry (IHC) to examine Girdin protein expression in tissue sections of surgically resected tumors obtained from esophageal cancer patients in our institution (**Table 1**). The results showed varying degrees of Girdin expression between cancer cells (**Fig. 1D**). We also examined Girdin expression in biopsy samples taken from the patients before treatment and stratified their outcome by a scoring system based on Girdin expression levels determined by IHC, but found no correlation between the patients' survival and Girdin expression (**Fig. 1E**). Interestingly, even in the same tumor, Girdin expression was different between different tumor lesions, as often observed for other cancer cell markers (**Fig. 1D**). We speculated that the intra-tumor heterogeneity of Girdin expression and its involvement in cancer cell sensitivity to anticancer therapeutics could confound the analysis based on simple measurement of Girdin mRNA and protein expression levels in whole tumors.

3.2 High Girdin expression is associated with a high sensitivity to UVC irradiation

Given the heterogeneous expression of Girdin between tumor cells and its unclear prognostic significance in esophageal cancer, we speculated that Girdin may be involved in tumor cell sensitivity to anticancer therapeutics. A previous study had reported that Girdin expression regulates the sensitivity of colon cancer cells to the chemotherapeutic drug oxaliplatin (35). In this study, we examined the significance of Girdin expression in cancer cells' sensitivity to DNA damage induced by radiotherapy. As a model of radiotherapy, we subjected cancer cells to high dose UVC irradiation (20-100 J/m^2) that produces pyrimidine

dimers and double stranded DNA breaks that contribute to the induction of apoptotic cell death (36). We first investigated two esophageal cancer cell lines KYSE140 and KYSE150 (32) that exhibited high and low levels of endogenous Girdin, respectively, and found that Girdin expression was not affected by UVC irradiation in both cell lines (**Fig. 2A**). We found that the number of cells that survived after UVC exposure, which was evaluated by colony-forming capacity, was higher in KYSE150 cells than KYSE140 cells (**Fig. 2B, C**). The data implied that Girdin expression may be associated with cancer cell sensitivity to UVC exposure.

To interrogate whether Girdin expression conferred sensitivity to UVC exposure, we attempted to exogenously overexpress Girdin by using lentiviral and retroviral expression systems. However, the large size of Girdin cDNA (5,500 bp) made it difficult to achieve high viral packaging efficiency. We therefore adopted the synergistic activation mediators (SAM) system (33) that permitted us to express an engineered CRISPR/Cas9 complex to augment endogenous Girdin expression by transcriptional activation of the Girdin gene (*CCDC88A*) locus in HeLa human cervical cancer cells (**Fig. 2D**). Western blot analysis showed successful overexpression (OE) of endogenous Girdin in HeLa cells (**Fig. 2E**). Although H2AX phosphorylation was comparable between control (C) and Girdin OE cells, Girdin OE cells exhibited high sensitivity to DNA damage as shown by a decreased capacity in colony formation after UVC irradiation (**Fig. 2E-G**).

3.3 HeLa cells overexpressing Girdin are vulnerable to UVC irradiation

Using Western blot analysis of UVC-irradiated HeLa cells that expressed high levels of endogenous Girdin, we found that they expressed higher levels of cleaved PARP1, a

marker of apoptosis, than did control cells (**Fig. 3A, B**). This was confirmed by immunofluorescent (IF) staining of control and Girdin OE HeLa cells with an antibody specific for cleaved PARP1 (**Fig. 3C, D**). Conversely, the knockdown of Girdin by siRNA-mediated RNA interference resulted in a significant decrease in cleaved PARP1 levels compared to control cells after UVC irradiation (**Fig. 3E-H**). Exogenous overexpression of Girdin in KYSE150 cells also resulted in an increase in cleaved PARP1 levels after UVC irradiation (**Fig. S1A, B**). Furthermore, KYSE140 cells, which express a higher level of Girdin, exhibited a higher sensitivity to UV exposure than KYSE150 cells with a low Girdin expression (**Fig. S1C**). These data suggested that Girdin expression is associated with the sensitivity of cancer cells to UVC-mediated DNA damage and subsequent cell apoptosis.

3.4 The Girdin-mediated increase in UVC sensitivity eliminates the DNA damage-protective effect of cell migration

In contrast to proliferating cells, migrating cells are significantly resistant to DNA damage-induced apoptosis (24, 25). Given the well-established roles of Girdin in cell migration (9, 11, 15, 16, 26), it was plausible to speculate that the observed effect of Girdin expression on UVC-induced apoptosis was attributed to an altered cell migratory response. To address this question, we scratched confluent monolayers of HeLa cells to induce directional cell migration, followed by UVC irradiation, Western blot analysis, and IF staining (**Fig. 4A**). In a control experiment, the cells were fixed immediately after the scratch and UVC irradiation without inducing cell migration (**Fig. 4A**). Throughout the

experiments, the cells were cultured with a low concentration of FBS (0.5%) in order to minimize their proliferation.

Consistent with the known pro-migratory role of Girdin, Girdin OE cells exhibited more rapid migration as assessed by the closure of the wounds made by scratching of cell monolayers (**Fig. 4B**). Interestingly, IF staining of migrating HeLa cells showed an uneven distribution of cleaved PARP1-positive cells in the scratched monolayers after UVC irradiation (**Fig. 4C**). We therefore counted and quantified cleaved PARP1-positive apoptotic cells in 3 groups of migrating cells: leading cells in the front line of migrating cell groups (the first row of cells; L), the most anterior cells including the leading cells (300 μm in distance from the front line; zone 1), and cells behind the zone 1 cells (300 – 600 μm from the front line; zone 2) (**Fig. 4A, C**). In migrating cells, but not non-migrating cells, the frequency of apoptotic cells in the L group was significantly lower than those in zones 1 and 2, further confirming that migrating cells are resistant to DNA damage-induced apoptosis (**Fig. 4D**, left and middle panels). Interestingly, Girdin OE cells showed similar proportions of apoptotic cells in L, zone 1 and zone 2 groups, and an increase in the numbers of apoptotic cells across all the groups (**Fig. 4D**, right panel). Conversely, the knockdown of Girdin equalized the distribution of apoptotic cells without increasing the numbers of those cells across all the groups (**Fig. 4E**). These data suggested that Girdin OE increases the sensitivity of cancer cells to UVC-induced DNA damage even when they migrate, and eliminates the DNA damage-protective effect of cell migration.

3.5 Altered cell cycle distribution in Girdin OE cells

We next explored the mechanism by which high Girdin expression was linked to high sensitivity to DNA damage and subsequent apoptosis. To that end, we examined the cell cycle distribution of Girdin OE HeLa cells. Flow cytometric analysis of non-synchronized cells stained with PI showed that Girdin OE cells accumulated in G1 phase with a lower fraction in the S phase in both HeLa and the esophageal cancer cell line KYSE150 (**Fig. 5A, Fig. S1D, E**). This was confirmed by another set of experiments, in which we analyzed the cell cycle distribution using 5−ethynyl−2′−deoxyuridine (EdU) incorporation and PI staining (**Fig. S2A, B**). WST-1 assay showed statistically significant but marginal differences in cell proliferation between control and Girdin OE cells (**Fig. S2C**), suggesting that Girdin OE perturbs cell cycle distribution without affecting the length of the cell cycle.

Further flow cytometric analysis showed that the number of mitotic cells identified based on PI staining and their reactivity with anti-phospho histone H3 (Ser10) antibody was increased in Girdin OE cells compared to control cells (**Fig. 5B, C**). This was confirmed in synchronized HeLa cells in which cells were treated with nocodazole (60 ng/mL) for 16 h to generate a mitotic block, followed by shaking off to select for mitotic cells and replating them to release them from the block and induce progression to G1 phase (34) (**Fig. 5D**). Flow cytometric analysis showed that the percentage of cells that remained arrested in M phase 90 min after the release was higher in Girdin OE cells than in control cells (**Fig. 5E**). The mitotic delay in Girdin OE cells compared to control cells was also manifest when the cells were arrested by double thymidine block at the G1/S boundary and then released to reach a peak at mitosis (**Fig. S3A, B**). These data showed that high expression of Girdin was associated with the dysregulation of the cell cycle distribution with longer G1 and M phases.

3.6 Basal dysregulation of the cell cycle and p53 activation may increase apoptosis in Girdin OE cells after UVC irradiation

We next found that the exposure of control cells to UVC irradiation resulted in the accumulation of cells in the G1 phase of the cell cycle (**Fig. 5F**), consistent with previous studies (37). Although this effect was also observed in Girdin OE cells, the most remarkable change found in Girdin OE cells after UVC irradiation was a decrease in the number of cells in the G2/M phase (**Fig. 5F**). The data suggested that the longer M phase in Girdin OE cells contributed to their vulnerability to DNA damage and apoptosis. Previous studies have shown that p53 becomes stabilized and activated after prolonged mitosis and mitotic arrest to inhibit cell growth (38). Consistent with this, Western blot analysis showed the activation of p53, but not that of another tumor suppressor, Rb, in Girdin OE cells before UVC irradiation, which became more apparent after the irradiation (**Fig. 5G**). Given the established roles of p53 in apoptosis following DNA damage, it is plausible that prolonged mitosis and concomitant p53 activation found in Girdin OE cells may sensitize cells to subsequent UVC-induced DNA damage. The activation of p53 was also found in the esophageal cancer cell lines KYSE140 and KYSE150 exposed to UVC (**Fig. S1C**). However, it was not clear whether p53 activation levels correlated with Girdin expression in those cells, suggesting that Girdin-mediated sensitization of cancer cells to UVC irradiation may involve multiple mechanisms and not be simply explained by p53.

3.7 Girdin OE increases the expression level of Mad2, a mitotic spindle checkpoint protein, in HeLa cells

The phenotype observed in Girdin OE cells was not likely to be explained by any previously identified Girdin-interacting protein, including actin filaments, the cell polarity regulator Par-3, disrupted-in-schizophrenia 1 (DISC1) or α subunits of trimeric G proteins (9, 10, 11, 39), or cellular processes that Girdin is involved in. It was intriguing to find an increase in Cdk5-dependent phosphorylation of Girdin in UVC-irradiated Girdin OE cells (**Fig. S4**), but it was difficult to interpret the role of the Cdk5-Girdin pathway in the context of UVC-mediated apoptotic cell death and Girdin-mediated mitotic delay. We therefore searched for other mechanisms that involve Girdin to regulate cell cycle progression, and found that Mad2, a key component of the spindle checkpoint machinery that is crucial for anaphase onset in M phase (40-42), was highly upregulated in Girdin OE cells compared to control cells at both the protein and mRNA levels (**Fig. 6A, B**). It was noted that Mad2 expression was significantly increased in both non-synchronized and synchronized Girdin OE cells (**Fig. 6B-D**). Fractionation experiments showed that the Girdin OE-mediated increase in Mad2 expression was more prominent in the cytosolic fraction of cells in interphase but not M phase, suggesting a role of the aberrantly expressed Mad2 in dysregulating the progression of the cell cycle in interphase (**Fig. 6D**). However, an IF staining for tubulin proteins identified no apparent disorganization nor alignment of the microtubules in interphase, but revealed that the number of metaphase or early anaphase cells that undergo multipolar division was increased in Girdin OE cells compared to control cells (**Fig. S5A, B**). Thus, it may be possible that Girdin OE induces mitotic delay by interfering with Mad2-mediated regulation of the spindle checkpoint machinery. A correlation between Girdin and Mad2 expression was also observed in tissue samples of a human esophageal cancer cohort available from the TCGA database (**Fig. 6E**). Although speculative, the data implied that Mad2 overexpression has a role in cell cycle dysregulation found in Girdin OE cells also in human cancer.

3.8 No significant statistical correlation was found between Girdin expression and response to radiation therapy in esophageal cancer

The findings described above were obtained with cultured cancer cells. To extend those data, we asked whether Girdin expression was correlated with the response to radiotherapy in cancer patients. Given the availability of both pre- and post-radiation tissue samples in a cohort of esophageal cancer patients (N = 28) in our institution, we used IHC to examine Girdin expression in the biopsies and surgical samples that were obtained both pre- and post-radiation, respectively (**Table 1, Fig. 1E, Fig. S6A, B**). We adopted several scoring systems including one developed in a previous study (17) to evaluate Girdin expression levels in human esophageal cancer. The data from both pre- or post-radiation samples, however, did not show a correlation between Girdin expression levels and histopathological evaluation of the response to radiation therapy (**Fig. S6A, B**). Although not conclusive (given the limited number of samples), it seems that elevated Girdin expression alone does not confer sensitivity to radiotherapy, at least in esophageal cancer patients. That suggests a far more complex mechanism of radiosensitivity or the need to stratify and select patients who will benefit from elevated Girdin expression.

4. Discussion

The present study showed an unexpected link between Girdin (a regulator of cell migration in development and cancer progression) and the sensitivity of cancer cells to DNA damage.

In contrast to the general view that migratory cells are resistant to DNA damage, HeLa cells that expressed high levels of Girdin exhibited increased sensitivity to UVC-mediated DNA damage and subsequent apoptosis (**Fig. 6F**). Pathological analysis showed extensive intra-tumor heterogeneity of Girdin expression, supporting the view that the sensitivity to DNA damage is also variable among cancer cells. Together with previous studies that have shown a crucial role of Girdin in cancer cell invasion and metastasis, the data reveal complex effects of Girdin expression on cancer patients' outcomes.

Previous studies of Girdin function, including those in our laboratory, have shown that Girdin is involved in many cellular processes, including actin reorganization, cell migration, polarization, proliferation and metabolism (9, 11, 12, 30). Studies of Girdin-deficient mice indicated that a major *in vivo* role of Girdin is the regulation of collective migration and proper positioning of newborn neurons in developing and young adult brains (14, 39, 43). Given the results obtained from Girdin-deficient mice, the results of Bhandari *et al.* were unexpected. They showed that Girdin functions as a regulator of the migration-proliferation dichotomy (23). The migration-proliferation dichotomy is a hallmark of normal as well as cancer cells that cell migration and proliferation do not occur simultaneously (22). This mechanism helps to explain the resistance of migratory cancer cells to various cytotoxic therapeutics that target proliferating cells (24, 25). Girdin promotes migration upon phosphorylation by Cdk5, whereas nonphosphorylated Girdin promotes proliferation (23). Our present study added a new dimension to Girdin function, i.e., that high expression of Girdin enhances the vulnerability of cancer cells to DNA damage. These results seem to contradict the previous finding that Girdin promotes cell migration and cancer progression but may provide opportunities for therapeutic intervention if Girdin expression could be manipulated in human malignancies.

An unexpected but intriguing finding of the present study was that overexpression of Girdin delayed G1 and M phases, both of which are sensitive to UVC (**Fig. 6F**). This might contribute to the increased sensitivity of Girdin OE cells to DNA damage. Our analysis identified that Mad2 expression was transcriptionally upregulated in Girdin OE cells, which may explain the dysregulation of the cell cycle in Girdin OE cells. We have not yet, however, delved into the detailed mechanisms underlying this observation. Given the role of Mad2 in prolonging checkpoint arrest caused by DNA damage (44), it is plausible that elevated Girdin and Mad2 are both involved in the dysregulation of the cell cycle and subsequent UVC-induced DNA damage and cell death.

Our clinicopathological analysis showed no correlation of Girdin expression levels with the response to radiation therapy in a cohort of esophageal cancer patients. This finding is inconsistent with the hypothesis proposed in the present study. Alternatively, it suggests a complex compensatory mechanism underlying the resistance of cancer cells to radiation therapy. Expression of Girdin in various compartments of the tumor microenvironment including tumor vessels and cancer-associated fibroblasts must be considered (27). Further studies will be needed to demonstrate the *in vivo* significance of the present study, and care should be taken in developing new therapeutics that target pathways involving Girdin.

One limitation of this study can be attributed to the sources of cells used in the analyses. Given the availability of pre- and post radiation tissue samples, we examined tissue samples obtained from patients with esophageal cancer. However, we mainly relied on a HeLa cell line for *in vitro* studies because it had been widely used for cell cycle analysis. It is plausible that the mechanisms and frequencies of the acquisition of resistance to cytotoxic therapies are different across cancer types. The generality of the findings of this study,

therefore, must be confirmed by further studies in the future. Another concern regarding the present study is that it was based on the use of UVC and not ionizing radiation such as that used clinically, i.e., X-ray photon beams. Considering that the high dose of UVC adopted in this study resulted in double-strand DNA breaks (DSB) similar to the DNA damage caused by ionizing radiations, we believe that the present findings recapitulate the effects of X-ray irradiation therapy and other radiation therapies (45). Further studies on tumor mouse models with genetically engineered expression of Girdin could provide insights into the biological significance of Girdin expression in cancer cell sensitivity to radiation therapies.

Acknowledgments

We gratefully thank Kaori Ushida and Maki Takagishi for support in immunostaining and Yasuyuki Mizutani and Minoru Tanaka for support in flow cytometry. This work was supported by a Grant-in-Aid for Scientific Research (S) (26221304 to M.T.) and a Grant-in-Aid for Scientific Research (B) (18H02638 to A.E.) commissioned by the Ministry of Education, Culture, Sports, Science and Technology of Japan; AMED-CREST (Japan Agency for Medical Research and Development, Core Research for Evolutional Science and Technology; 19gm0810007h0104 and 19gm1210008s0101 to A.E.); and the Project for Cancer Research and Therapeutic Evolution (P-CREATE) from AMED (19cm0106332h0002 to A.E.).

Conflict of interest

No potential conflicts of interest were disclosed.

ORCID

Atsushi Enomoto, http://orcid.org/0000-0002-9206-6116

Masahide Takahashi, https://orcid.org/0000-0002-2803-2683

References

1. Hanahan, D. & Weinberg, R.A. Hallmarks of cancer: The next generation. Cell 2011;144:646–674.

2. Barker, H., Paget, J., Khan, A. et al. The tumour microenvironment after radiotherapy: mechanisms of resistance and recurrence. Nat Rev Cancer 2015;15: 409–425.

3. Frosina G. DNA repair and resistance of gliomas to chemotherapy and radiotherapy. Mol Cancer Res 2009;7:989–999.

4. Musgrove, E., Sutherland, R. Biological determinants of endocrine resistance in breast cancer. Nat Rev Cancer 2009;9:631–643.

5. Marusyk, A., Almendro, V. & Polyak, K. Intra-tumour heterogeneity: a looking glass for cancer?. Nat Rev Cancer 2012;12:323–334.

6. Fisher, R., Pusztai, L. & Swanton, C. Cancer heterogeneity: implications for targeted therapeutics. Br J Cancer 2013;108:479–485.

7. Rich JN. Cancer stem cells in radiation resistance. Cancer Res 2007;67:8980–8984.

8. Aguirre-Ghiso, J. Models, mechanisms and clinical evidence for cancer dormancy. Nat Rev Cancer 2007;7:834–846.

9. Enomoto A, Murakami H, Asai N, et al. Akt/PKB regulates actin organization and cell motility via Girdin/APE. Dev Cell 2005;9:389–402

10. Le-Niculescu H, Niesman I, Fischer T, DeVries L, Farquhar MG. Identification and characterization of GIV, a novel Gαi/s-interacting protein found on COPI, endoplasmic reticulum-Golgi transport vesicles. J Biol Chem 2005;280:22012–20.

11. Ohara K, Enomoto A, Kato T, et al. Involvement of Girdin in the determination of cell polarity during cell migration. PLoS One 2012;7:e36681.

12. Weng L, Enomoto A, Miyoshi H, et al. Regulation of cargo-selective endocytosis by dynamin 2 GTPase-activating protein girdin. EMBO J 2014;33:2098–2112.

13. Garcia-Marcos M, Ghosh P, Farquhar MG. GIV/Girdin transmits signals from multiple receptors by triggering trimeric G protein activation. J Biol Chem 2015;290:6697–6704.

14. Wang Y, Kaneko N, Asai N, et al. Girdin is an intrinsic regulator of neuroblast chain migration in the rostral migratory stream of the postnatal brain. J Neurosci. 2011;31:8109–8122.

15. Wang X, Enomoto A, Asai N, et al. Collective invasion of cancer: Perspectives from pathology and development. Pathol Int 2016;66:183-192.

16. Wang X, Enomoto A, Weng L, et al. Girdin/GIV regulates collective cancer cell migration by controlling cell adhesion and cytoskeletal organization. Cancer Sci 2018;109:3643–3656.

17. Shibata T, Matsuo Y, Shamoto T, et al. Girdin, a regulator of cell motility, is a potential prognostic marker for esophageal squamous cell carcinoma. Oncol Rep 2013;29:2127–2132.

18. Dunkel Y, Diao K, Aznar N, et al. Prognostic impact of total and tyrosine phosphorylated GIV/Girdin in breast cancers. FASEB J 2016;30:3702–3713.

19. Jiang P, Enomoto A, Jijiwa M, et al. An actin-binding protein Girdin regulates the motility of breast cancer cells. Cancer Res 2008;68:1310–1318.

20. Garcia-Marcos M, Jung BH, Ear J, Cabrera B, Carethers JM, Ghosh P. Expression of GIV/Girdin, a metastasis-related protein, predicts patient survival in colon cancer. FASEB J 2011;25:590–599.

21. Ghosh P, Tie J, Muranyi A, et al. Girdin (GIV) Expression as a Prognostic Marker of Recurrence in Mismatch Repair-Proficient Stage II Colon Cancer. Clin Cancer Res 2016;22:3488–3498.

22. Ghosh P, Beas AO, Bornheimer SJ, et al. A Gαi-GIV molecular complex binds epidermal growth factor receptor and determines whether cells migrate or proliferate. Mol Biol Cell 2010;21:2338–2354.

23. Bhandari D, Lopez-Sanchez I, To A, et al. Cyclin-dependent kinase 5 activates guanine nucleotide exchange factor GIV/Girdin to orchestrate migration-proliferation dichotomy. Proc Natl Acad Sci U S A 2015;112:E4874–E4883.

24. Joy AM, Beaudry CE, Tran NL, et al. Migrating glioma cells activate the PI3-K pathway and display decreased susceptibility to apoptosis. J Cell Sci 2003;116:4409–4417.

25. Theys J, Jutten B, Habets R, et al. E-Cadherin loss associated with EMT promotes radioresistance in human tumor cells. Radiother Oncol 2011;99:392-397.

26. Kitamura T, Asai N, Enomoto A, et al. Regulation of VEGF-mediated angiogenesis by the Akt/PKB substrate Girdin. Nat Cell Biol 2008;10:329-337.

27. Yamamura Y, Asai N, Enomoto A, et al. Akt-Girdin signaling in cancer-associated fibroblasts contributes to tumor progression. Cancer Res 2015;75:813–823.

28. Choi JS, Kim KH, Oh E, et al. Girdin protein expression is associated with poor prognosis in patients with invasive breast cancer. Pathology 2017;49:618–626.

29. Natsume A, Kato T, Kinjo S, et al. Girdin maintains the stemness of glioblastoma stem cells. Oncogene 2012;31:2715-24.

30. Weng L, Han YP, Enomoto A, et al. Negative regulation of amino acid signaling by MAPK-regulated 4F2hc/Girdin complex. PLoS Biol 2018;16:e2005090.

31. Han YP, Enomoto A, Shiraki Y, et al. Significance of low mTORC1 activity in defining the characteristics of brain tumor stem cells. Neuro Oncol 2017;19:636–647.

32. Shimada Y, Imamura M, Wagata T, Yamaguchi N, Tobe T. Characterization of 21 newly established esophageal cancer cell lines. Cancer 1992;69:277–284.

33. Konermann S, Brigham MD, Trevino AE, et al. Genome-scale transcriptional activation by an engineered CRISPR-Cas9 complex. Nature 2015;517:583–588.

34. Jackman J, O'Connor PM. Methods for synchronizing cells at specific stages of the cell cycle. Curr Protoc Cell Biol 2001;Chapter 8:Unit 8.3.

35. Zhang YJ, Li AJ, Han Y, Yin L, Lin MB. Inhibition of Girdin enhances chemosensitivity of colorectal cancer cells to oxaliplatin. World J Gastroenterol 2014;20:8229–8236.

36. Takasawa R, Nakamura H, Mori T, Tanuma S. Differential apoptotic pathways in human keratinocyte HaCaT cells exposed to UVB and UVC. Apoptosis 2005;10:1121–1130.

37. Di Leonardo A, Linke SP, Clarkin K, Wahl GM. DNA damage triggers a prolonged p53-dependent G1 arrest and long-term induction of Cip1 in normal human fibroblasts. Genes Dev 1994;8:2540–2551.

38. Fong CS, Mazo G, Das T, et al. 53BP1 and USP28 mediate p53-dependent cell cycle arrest in response to centrosome loss and prolonged mitosis. Elife 2016;5:e16270.

39. Enomoto A, Asai N, Namba T, et al. Roles of disrupted-in-schizophrenia 1-interacting protein girdin in postnatal development of the dentate gyrus. Neuron 2009;63:774–787.

40. Kallio M, Weinstein J, Daum JR, Burke DJ, Gorbsky GJ. Mammalian p55CDC mediates association of the spindle checkpoint protein Mad2 with the

cyclosome/anaphase-promoting complex, and is involved in regulating anaphase onset and late mitotic events. J Cell Biol 1998;141:1393–1406.

41. Fang G, Yu H, Kirschner MW. The checkpoint protein MAD2 and the mitotic regulator CDC20 form a ternary complex with the anaphase-promoting complex to control anaphase initiation. Genes Dev 1998;12:1871–1883.

42. Shah JV, Cleveland DW. Waiting for anaphase: Mad2 and the spindle assembly checkpoint. Cell 2000;103:997–1000.

43. Muramatsu A, Enomoto A, Kato T, et al. Potential involvement of kinesin-1 in the regulation of subcellular localization of Girdin. Biochem Biophys Res Commun. 2015;463:999-1005.

44. Dotiwala F, Harrison JC, Jain S, Sugawara N, Haber JE. Mad2 prolongs DNA damage checkpoint arrest caused by a double-strand break via a centromere-dependent mechanism. Curr Biol 2010;20:328–332.

45. Staszewski O, Nikolova T, Kaina B. Kinetics of gamma-H2AX focus formation upon treatment of cells with UV light and alkylating agents. Environ Mol Mutagen 2008;49:734–740.

Figure Legends

Figure 1. Prognostic value and intratumoral heterogeneity of Girdin expression in esophageal cancer

(A-C) Comparison of the overall survivals of Girdin-high and -low esophageal cancer samples available in the TCGA database. Ninety-six cases were classified according to Girdin expression, and overall survival of the cases was plotted by Kaplan-Meier analysis. Cut-off values of 25, 50, and 75% were selected and used to classify tumors as Girdin-low or -high.

(D) Representative images of tissue sections of 3 independent cases with esophageal cancer stained by Girdin antibody. The presence of Girdin-negative cells (white arrows) and Girdin-positive cells (yellow arrows) indicates intratumoral heterogeneity of Girdin expression.

(E) Comparison of the overall survivals of Girdin-high and -low esophageal cancer cases, who were diagnosed in Nagoya University Hospital. Biopsy samples taken from 29 cases were classified according to Girdin expression following the scoring system shown in left, and overall survival of the cases was plotted by the Kaplan-Meier analysis.

Figure 2. High Girdin expression is associated with increased vulnerability of cancer cells to UVC-mediated DNA damage

(A) KYSE140 and KYSE150 cell lines were exposed to UVC (100 J/m^2) and incubated for 3 h, followed by Western blot analysis with the indicated antibodies.

(B, C) Representative images of colonies of KYSE140 and KYSE150 cells formed 6 days after UVC irradiation are shown **(B)**. The locations of the colonies are indicated by the circles. In **(C)**, the surviving fractions (SF), which were calculated by dividing the numbers of colonies by the numbers of seeded cells that were multiplied by plating efficiencies, in 3 independent experiments were evaluated and quantified.

(D) Schematic illustration of the generation of Girdin OE HeLa cells by the CRISPR/sgRNA-directed synergistic activation mediator (SAM) system. TSS, transcription start site of the *CCDC88A* gene that encodes Girdin.

(E) Control (C) and Girdin OE HeLa cells were exposed to UVC irradiation (100 or 20 J/m2) for the indicated periods, followed by Western blot analysis.

(F, G) Control and Girdin OE HeLa cells exposed to UVC irradiation for 7 days, followed by colony formation assay. The surviving fractions in 3 independent experiments were evaluated and quantified.

Figure 3. High Girdin expression is associated with increased apoptosis of HeLa cells after UVC irradiation

(A, B) Control and Girdin OE HeLa cells were exposed to UVC irradiation (100 J/m2) and incubated for 3 h, followed by Western blot analysis **(A)**. The intensity of cleaved PARP1 signals was normalized against β-actin, and the data from 3 independent experiments is shown **(B)**.

(C, D) Control and Girdin OE HeLa cells were exposed to UVC irradiation (100 J/m2) and incubated for 3 h, followed by IHC for cleaved PARP1 **(C)**. The percentage of cleaved PARP1-positive cells was determined, and the data from 3 independent experiments is shown **(D)**.

(E-H) HeLa cells transfected with either control or Girdin siRNA were exposed to UVC irradiation and incubated for 3 h, followed by Western blot analysis **(E, F)** and IHC for cleaved PARP1 **(G, H)**.

Figure 4. Girdin-mediated sensitization of HeLa cells to UVC eliminates the protective effect of cell migration against DNA damage

(A) Schematic diagram of the experimental protocol to examine the effect of UVC irradiation on migrating cells. Monolayers of confluent HeLa cells on glass-based dishes (left, top) were scratched to initiate sheet migration into the wound (right, top), incubated for 16 h, exposed to UVC irradiation and incubated for 3 h (right, bottom). After fixation and IF staining, the leading cells in the front line of migrating cell group (L) and cells included in zones 1 and 2 were examined for cleaved PARP1 expression.

(B) Monolayers of control and Girdin OE HeLa cells were scratched to induce migration for 16 h, and the areas of wounds were measured by the ImageJ software and quantified. The percentages of wound closure in 24 images taken from 4 independent experiments were measured and quantified.

(C) A monolayer of HeLa cells was scratched to induce migration, followed by UVC exposure and IF staining, showing an uneven distribution of cleaved PARP1-positive cells across the cell groups.

(D-E) Monolayers of the indicated HeLa cells were subjected to UVC irradiation after cell migration for 16 h (migration (+)), or just immediately after scratching (migration (-)), followed by IF staining for cleaved PARP1 and quantification.

Figure 5. Girdin OE HeLa cells exhibit dysregulated cell cycle progression with prolonged G1 and M phases

(A) Flow cytometric analysis of non-synchronized control and Girdin OE HeLa cells. Cell cycle phase is shown at top.

(B, C) Non-synchronized control and Girdin OE HeLa cells were stained for phospho-histone H3 and then PI, followed by flow cytometric analysis. Representative flow histograms depicting mitotic fraction defined by arrows are shown in **(B)**, and the percentages of mitotic cells were quantified in **(C)**. Results are expressed as the means ± SD of 3 independent experiments.

(D, E) HeLa cells were synchronized at M phase by incubating the cells with nocodazole at 60 ng/mL for 16 h, collecting mitotic cells by mitotic shaking and replating **(D)**. Temporal changes in cell cycle distribution after replating were examined by flow cytometric analysis for PI stained cells **(E)**.

(F, G) Non-synchronized control and Girdin OE HeLa cells were exposed to UVC irradiation (100 J/m2) and incubated for 3 h, followed by cell cycle analysis by flow cytometric analysis of PI stained cells (F) and Western blot analysis with the indicated antibodies **(G)**.

Figure 6. Upregulation of Mad2 in Girdin OE cells and expression correlation between Girdin and Mad2

(A) mRNAs for Girdin (left) and Mad2 (right) isolated from control and Girdin OE cells were measured and quantified by quantitative PCR.

(B) Total cell lysates (Total) of control and Girdin OE HeLa cells were fractionated into nuclear and cytosolic fractions, followed by Western blot analysis with the indicated antibodies.

(C, D) HeLa cells were synchronized at M phase by incubating the cells with nocodazole at 60 ng/mL for 16 h, collecting mitotic cells by mitotic shake-off, and replating **(C)**. The expression of Girdin and Mad2 was examined by Western blot analysis after the fractionation of the attached cells and those in M phase (shake off and reseed) **(D)**.

(E) Correlation of Girdin and Mad2 expression in esophageal cancer samples (N =180) available in the TCGA database.

(F) Schematic model of the increased sensitivity to UVC in cancer cells with high Girdin expression. The data shown here suggest that the OE of Girdin perturbs cell cycle distribution with prolonged G1 and M phases and aberrant p53 activation but without

affecting the length of the cell cycle, which leads to an increase in sensitivity to DNA damage. The present study showed that the upregulation of the spindle checkpoint protein Mad2 in Girdin OE cells may be involved in dysregulated cell cycle progression. However, the detailed mechanism behind the observed vulnerability of Girdin OE cells to UVC is not clear at present. Given the known function of Girdin in promoting cell migration and the theory of migration-proliferation dichotomy, the present data reveals the complexity of cellular responses to high Girdin expression and its role in cancer progression.

List of Supporting Information

Supporting Figures: Fig. S1-6

Document S1 (Supporting Methods)

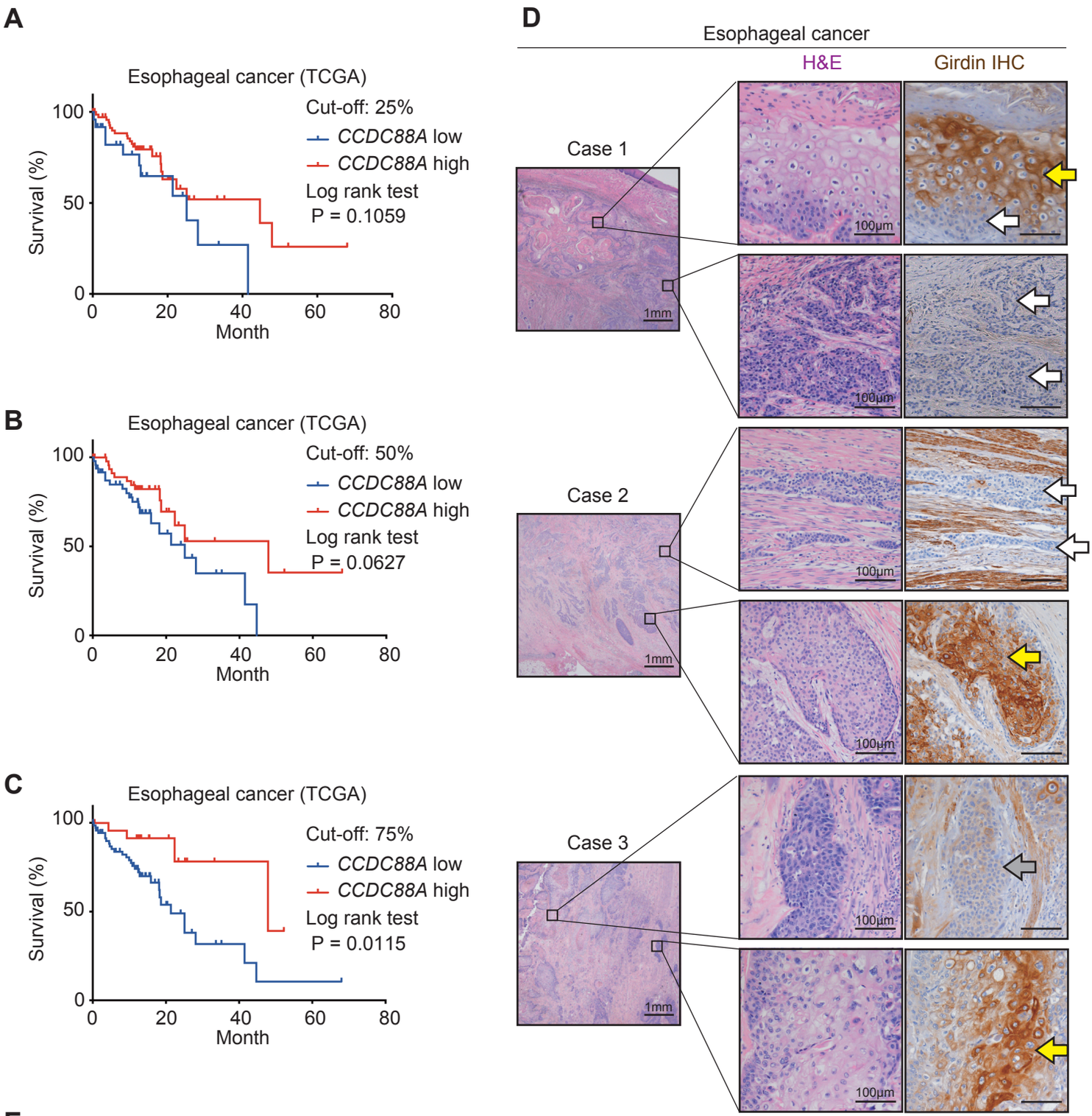

E

Biopsy sample (Pre-radiation samples)

Intensity score (IS)	
Score 0: Negative	Girdin low
Score 1: Weakly positive	
Score 2: Positive	Girdin high
Score 3: Strongly positive	

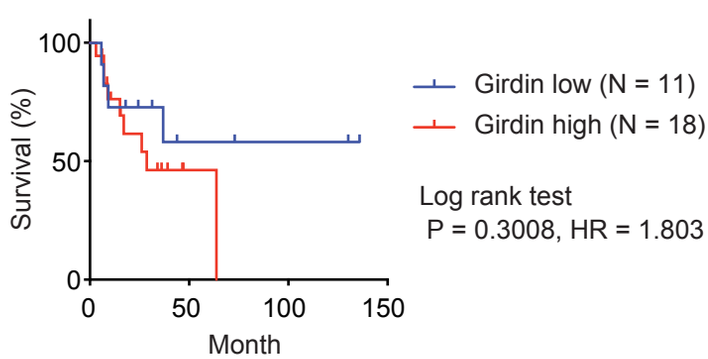

Figure 1

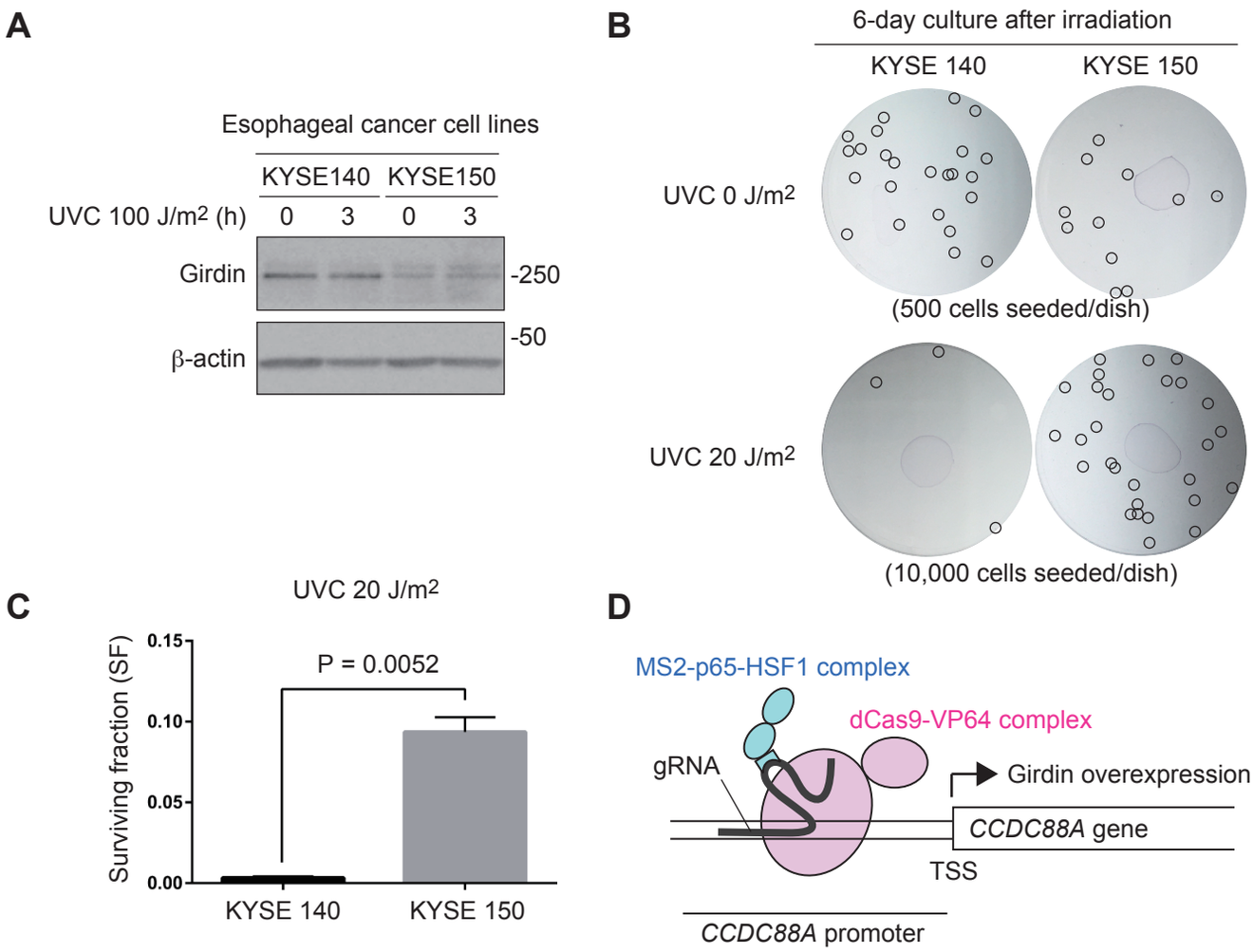
A
Esophageal cancer cell lines
KYSE140
KYSE150
UVC 100 J/m2 (h)
0
3
0
3
Girdin
-250
β-actin
-50
B
6-day culture after irradiation
KYSE 140
KYSE 150
UVC 0 J/m2
(500 cells seeded/dish)
UVC 20 J/m2
(10,000 cells seeded/dish)
C
UVC 20 J/m2
P = 0.0052
Surviving fraction (SF)
0.15
0.10
0.05
0.00
KYSE 140
KYSE 150
D
MS2-p65-HSF1 complex
dCas9-VP64 complex
gRNA
Girdin overexpression
CCDC88A gene
TSS
CCDC88A promoter
E
UVC 100 J/m2
UVC 20 J/m2
0
5
15
30
60
15
(min)
C
OE
Girdin
-250
β-actin
-42
Phospho-Histone H2AX
(Ser139)
-20
HeLa
F
HeLa
6-day culture after irradiation
Control
Girdin OE
UVC 0 J/m2
(500 cells seeded/dish)
UVC 20 J/m2
(1,000 cells seeded/dish)
G
UVC 20 J/m2
P = 0.0054
Surviving fraction (SF)
0.08
0.06
0.04
0.02
0.00
Control
Girdin OE

Figure 2

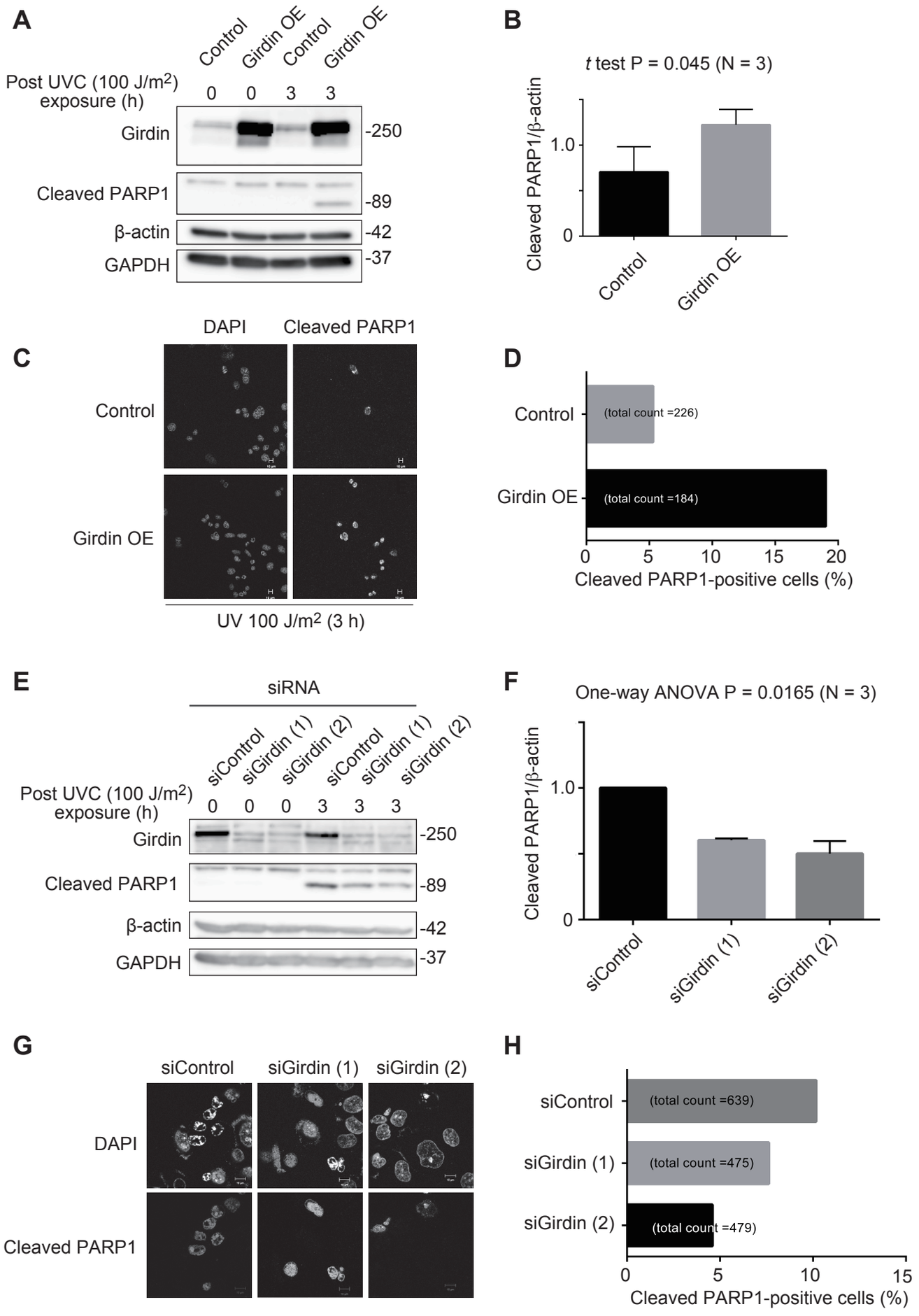
A
Control
Girdin OE
Control
Girdin OE
Post UVC (100 J/m2) exposure (h)
0 0 3 3
Girdin
-250
Cleaved PARP1
-89
β-actin
-42
GAPDH
-37
B
t test P = 0.045 (N = 3)
Cleaved PARP1/β-actin
1.0
0
Control
Girdin OE
C
DAPI
Cleaved PARP1
Control
Girdin OE
UV 100 J/m2 (3 h)
D
Control
(total count =226)
Girdin OE
(total count =184)
0 5 10 15 20
Cleaved PARP1-positive cells (%)
E
siRNA
siControl
siGirdin (1)
siGirdin (2)
siControl
siGirdin (1)
siGirdin (2)
Post UVC (100 J/m2) exposure (h)
0 0 0 3 3 3
Girdin
-250
Cleaved PARP1
-89
β-actin
-42
GAPDH
-37
F
One-way ANOVA P = 0.0165 (N = 3)
Cleaved PARP1/β-actin
1.0
0
siControl
siGirdin (1)
siGirdin (2)
G
siControl
siGirdin (1)
siGirdin (2)
DAPI
Cleaved PARP1
H
siControl
(total count =639)
siGirdin (1)
(total count =475)
siGirdin (2)
(total count =479)
0 5 10 15
Cleaved PARP1-positive cells (%)

Figure 3

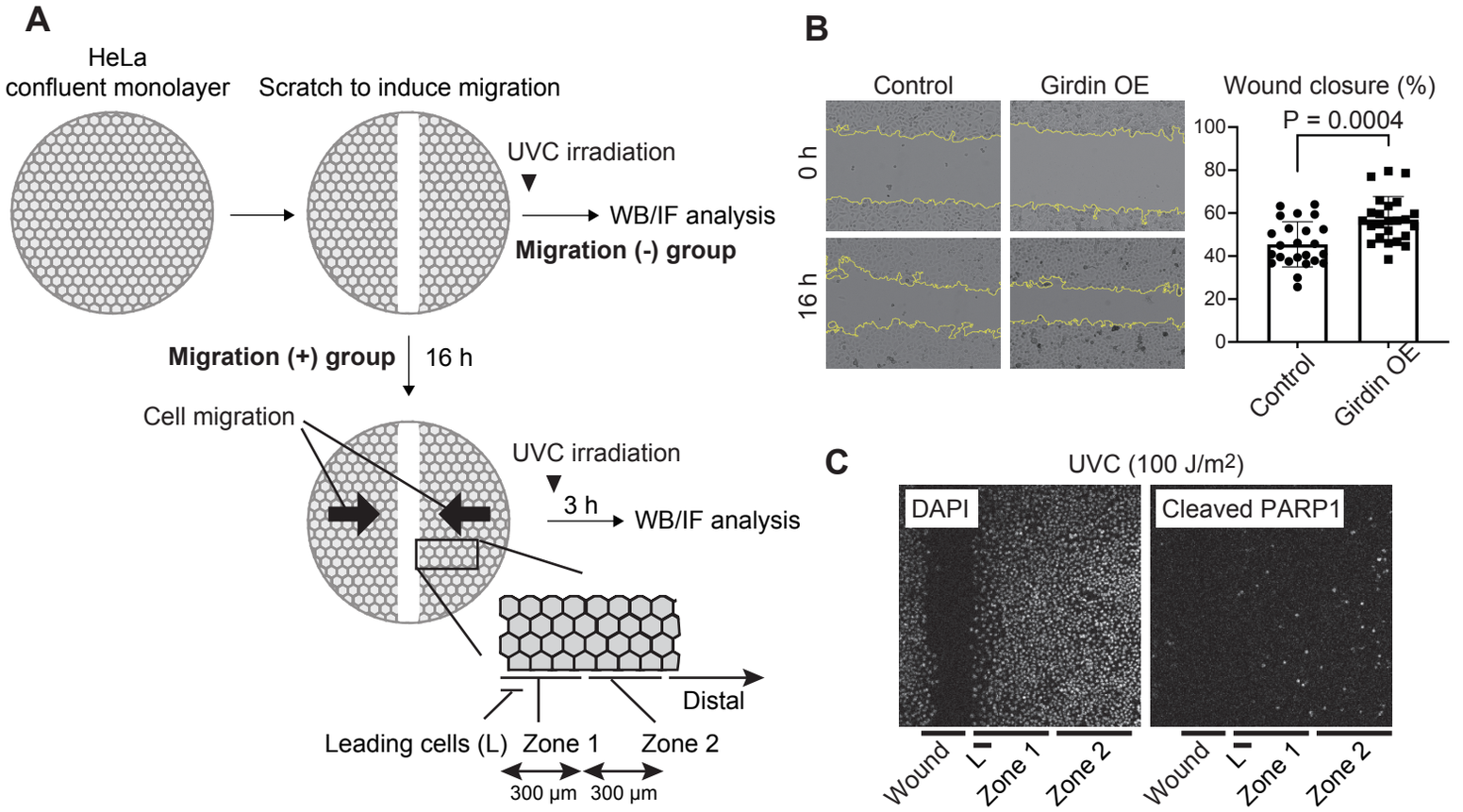
A
HeLa
confluent monolayer
Scratch to induce migration
UVC irradiation
WB/IF analysis
Migration (-) group
Migration (+) group
16 h
Cell migration
UVC irradiation
3 h
WB/IF analysis
Distal
Leading cells (L)
Zone 1
Zone 2
300 µm
300 µm
B
Control
Girdin OE
0 h
16 h
Wound closure (%)
P = 0.0004
Control
Girdin OE
C
UVC (100 J/m2)
DAPI
Cleaved PARP1
Wound
L
Zone 1
Zone 2
D
Migration (-)
Migration (+)
Control
Girdin OE
One-way ANOVA P = 0.60
One-way ANOVA P < 0.001
One-way ANOVA P = 0.45
Cleaved PARP1-positive cells (%)
Leading cells (L)
Zone 1
Zone 2
E
Migration (+)
siControl
siGirdin (1)
siGirdin (2)
One-way ANOVA P < 0.001
One-way ANOVA P = 0.16
Cleaved PARP1-positive cells (%)
Leading cells (L)
Zone 1
Zone 2
Distal

Figure 4

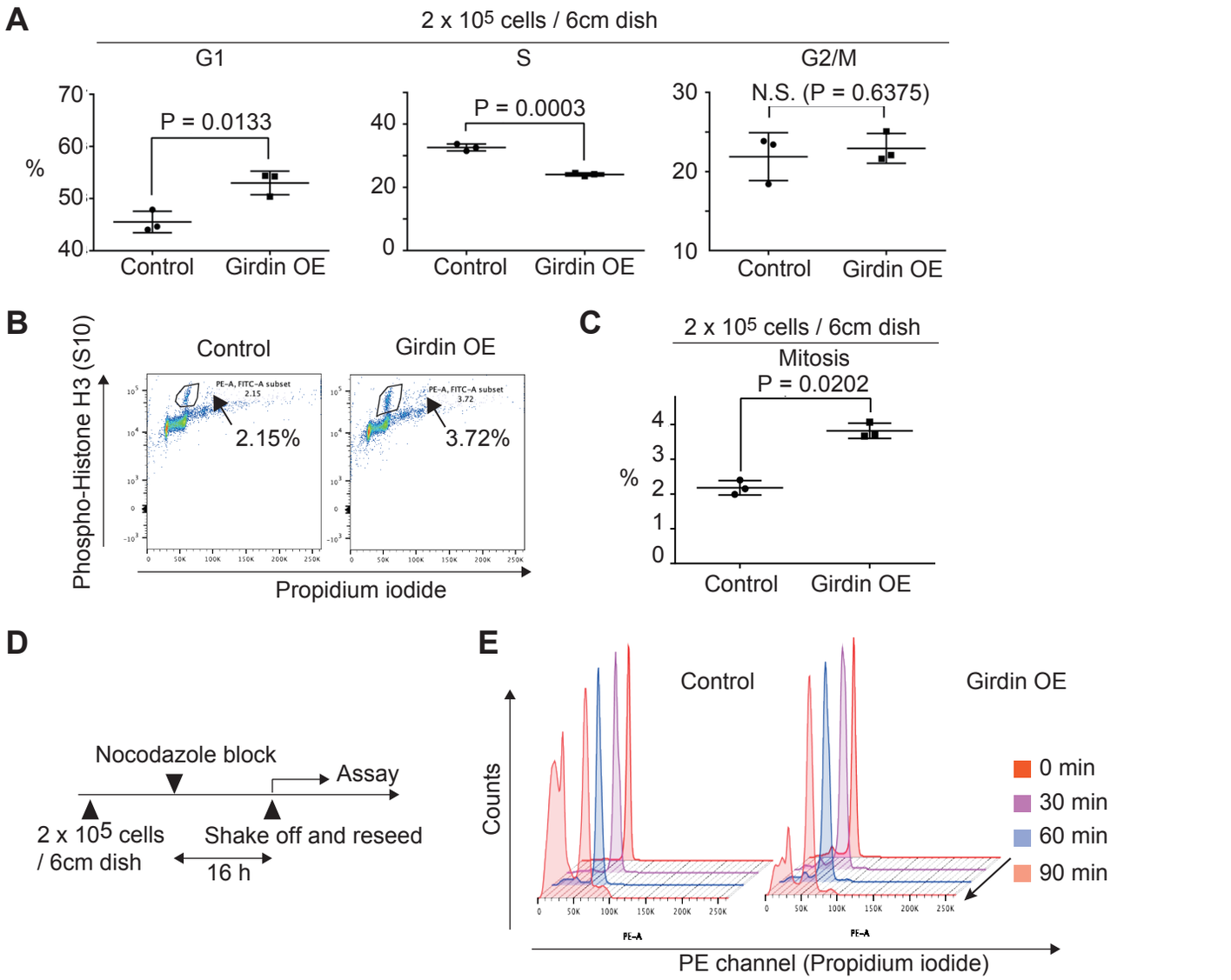
A
2 x 10^5 cells / 6cm dish
G1
S
G2/M
P = 0.0133
P = 0.0003
N.S. (P = 0.6375)
%
Control
Girdin OE
B
Control
Girdin OE
Phospho-Histone H3 (S10)
2.15%
3.72%
Propidium iodide
C
2 x 10^5 cells / 6cm dish
Mitosis
P = 0.0202
%
Control
Girdin OE
D
Nocodazole block
Assay
2 x 10^5 cells / 6cm dish
Shake off and reseed
16 h
E
Control
Girdin OE
Counts
0 min
30 min
60 min
90 min
PE channel (Propidium iodide)
F
2 x 10^5 cells / 6cm dish
Control
Girdin OE
G1
S
G2/M
P=0.0112
N.S. (P=0.0524)
N.S. (P=0.1994)
N.S (P=0.2905)
N.S. (P=0.0663)
P=0.0237
UVC (-)
UVC 100 J/m2
G
Control
Girdin OE
UVC (100 J/m2)
Girdin
Cleaved PARP1
Phospho-H2AX Ser15
Phospho-p53 Ser15
p53
Phospho-Rb Ser795
Rb
Phospho-Histone H3 (S10)
Histone H3
β-Actin
-250
-100
-15
-50
-50
-100
-100
-15
-15
-50

Figure 5

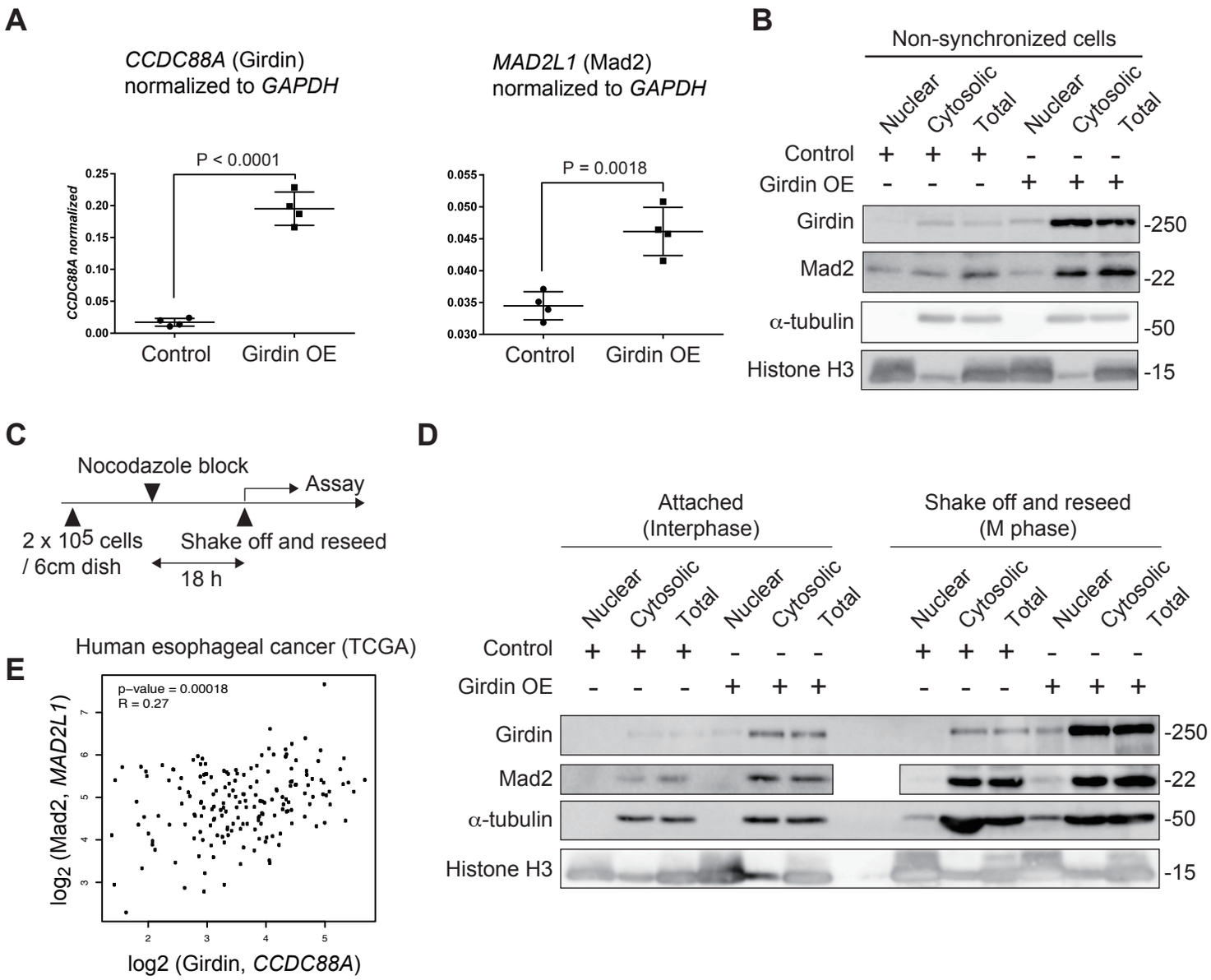
A
CCDC88A (Girdin) normalized to GAPDH
P < 0.0001
CCDC88A normalized
Control
Girdin OE
MAD2L1 (Mad2) normalized to GAPDH
P = 0.0018
Control
Girdin OE
B
Non-synchronized cells
Nuclear
Cytosolic
Total
Control
Girdin OE
Girdin
Mad2
α-tubulin
Histone H3
-250
-22
-50
-15
C
Nocodazole block
Assay
2 x 10^5 cells / 6cm dish
Shake off and reseed
18 h
D
Attached (Interphase)
Shake off and reseed (M phase)
E
Human esophageal cancer (TCGA)
p–value = 0.00018
R = 0.27
log2 (Mad2, MAD2L1)
log2 (Girdin, CCDC88A)
F
Cancer cell heterogenetiy
Girdin low
Girdin high (Girdin OE)
Cell migration
Actin remodeling
Mechanism?
Mad2 upregulation
M
G2
G1
S
p53
P
UVC
G1 arrest and DNA damage repair
Apoptosis

Figure 6

Table 1. Clinicopathological characteristics of esophageal cancer patients analyzed in the current study

Characteristics		Total	Girdin-low	(%)	Girdin-high	(%)	χ^2 test *P* value
Number		29	11	(37.9)	18	(62.1)	
Age (years)	< 65	70	8	(27.6)	8	(27.6)	0.1373
	≥ 65	130	3	(10.3)	10	(34.5)	
Sex	Male	24	8	(27.6)	16	(55.2)	0.2636
	Female	5	3	(10.3)	2	(6.9)	
Alcohol intake	No	9	2	(6.9)	7	(24.1)	0.2422
	Yes	20	9	(31.0)	11	(37.9)	
Brinkman index	< 1000	24	9	(31.0)	15	(51.7)	0.9165
	≥ 1000	5	2	(6.9)	3	(10.3)	
Tumor location	Cervix	1	1	(3.4)	0	(0.0)	0.3145
	Upper	7	3	(10.3)	4	(13.8)	
	Middle	18	7	(24.1)	11	(37.9)	
	Lower	3	0	(0.0)	3	(10.3)	
Histological grade	Grade 1	8	2	(6.9)	6	(20.7)	0.2284
	Grade 2	17	6	(20.7)	11	(37.9)	
	Grade 3	4	3	(10.3)	1	(3.4)	
Clinical stage	Ⅰ	2	1	(3.4)	1	(3.4)	0.9849
	Ⅱ	3	1	(3.4)	2	(6.9)	
	Ⅲ	16	6	(20.7)	10	(34.5)	
	Ⅳ	8	3	(10.3)	5	(17.2)	

Complex roles of the actin-binding protein Girdin/GIV in DNA damage-induced apoptosis of cancer cells

Chen *et al.*

Supporting Methods

TCGA data analysis

By using the GEPIA (Gene Expression Profiling Interactive Analysis) web server (http://gepia.cancer-pku.cn), the mRNA expression data of esophageal carcinoma samples from the The Cancer Genome Atlas (TCGA) database was analyzed.

Immunohistochemistry (IHC) studies

Formalin-fixed and paraffin-embedded tissue sections were deparaffinized, subjected to antigen retrieval using Target-Retrieval Solution (Dako) at pH 6 or 9 for 30 min, and stained using conventional procedures.

Colony formation assay

Colony formation assay was performed as described elsewhere (Franken *et al*., Nat Protocol 1:2315, 2006). Exponentially growing cells were plated on 60-mm dishes with appropriate numbers of cells per dish. Six hours after plating, cells were confirmed to be attached by using a microscope and then exposed to UVC and incubated for 6 days to allow colony formation. The cells were fixed for 30 min using 100% methanol and exposed to a May Grunwald Stain solution (MG500, Sigma-Aldrich) for 30 min. Dishes

were rinsed with tap water and dried at room temperature. Counting of clones was performed on the following day.

Transient transfection and RNA interference

Transient transfections of siRNA or plasmid were performed by Lipofectamine 2000 following the manufacturer's instructions. The siRNAs including control siRNA were purchased from Qiagen (Venlo, Netherlands). The target sequences of the siRNAs were Girdin (1), 5′-AAGAAGGCTTAGGCAGGAATT-3′ and Girdin (2), 5'-AACCAGGTCATGCTCCAAATT-3'.

Plasmids

The details of the Girdin-V5 expression plasmid were described previously (ref. 39, Enomoto *et al*., Neuron 63:774–787, 2009).

Total RNA extraction and real-time qPCR

Total RNA was extracted using an RNeasy Plus Mini Kit (Qiagen) according to the manufacturer's instruction. cDNA was synthesized from 2 μg total RNA using ReverTra Ace qPCR RT Master Mix (TOYOBO, Tokyo, Japan). Real time qPCR was performed using a TaqMan Gene Expression assay (Thermo Fisher Scientific) on an Mx3000P qPCR System (Agilent Technologies). Gene expression levels were analyzed using the 2-ΔΔCt method and normalized relative to the expression levels of the housekeeping gene *GAPDH*. The TaqMan probes are listed as follows: human

CCDC88A, Hs00214014_m1; human *MAD2L1*, Hs01554513_g1; human *GAPDH*, Hs02758991_g1. All experiments were performed in triplicates.

Cell proliferation assay

Cell proliferation was measured with a Cell Proliferation Reagent WST-1 kit (Roche Diagnostics, Darmstadt, Germany) according to the manufacturer's instruction. Cells (0.1 mL) were seeded in each well at a concentration of 10^4 cells/mL on 96-well plates. After the indicated incubation periods, 10 μL/well Premix WST-1 was added. Cells were incubated for 3 h and the absorbance was measured at a wavelength of 450 nm on a POWERSCAN4 (BioTek, Winooski, VT).

Flow cytometric analysis for the detection of apoptotic cells

For the analysis of apoptosis, cells were collected and fixed with 4% paraformaldehyde for 15 min, followed by incubation with permeabilization buffer (0.2% Triton™ X-100) for 15 min. Cells were incubated with anti-cleaved PARP1 antibody (Abcam) for 1 h at room temperature, washed with PBS, and incubated with Alexa Fluor 488-conjugated rabbit anti-mouse IgG (Thermo Fisher Scientific) for 30 min at room temperature in the dark.

Immunofluorescent (IF) staining

Cells were fixed with 4% paraformaldehyde for 15 min, permeabilized with 0.15% Triton X-100 for 30 min, and blocked with 10% goat serum (Nichirei Biosciences,

Tokyo, Japan) for 30 min. Cells were stained with anti-cleaved PARP1 antibody overnight at 4°C. After 3 washes with PBS, the cells were incubated with Alexa Fluor 488-conjugated goat anti-mouse IgG (Thermo Fisher Scientific) for 1 h. DAPI was used to stain the cell nuclei. For the staining of microtubules, cells were seeded at poly-D-lysine-coated 35 mm glass base dishes (Iwaki, Tokyo, Japan). The next day, cells were fixed with methanol for 5 min at -20ºC, followed by blocking with 10% goat serum for 1 h at room temperature. Cells were incubated with anti-α-Tubulin and anti-γ-Tubulin antibodies for 1 h at room temperature, washed with PBS, and incubated with Alexa Fluor 488-conjugated goat anti-mouse IgG and Alexa Fluor 488-conjugated goat anti-rabbit IgG for 45 min at dark.

Microscopic imaging

For cell migration assays, the fluorescence of cleaved PARP1 and DAPI was detected using a BZ-X710 microscope (Keyence, Osaka, Japan) with a CFI Plan Apochromat 20X/0.75 objective lens (Nikon, Tokyo, Japan). Images were collected using BX-Viewer software (Keyence). For other imaging assay, images were obtained by an LSM 700 confocal microscope equipped with a Plan Apochromat 63X/1.4 Oil DIC objective lens (Carl Zeiss AG, Oberkochen Germany). Images were collected using ZEISS ZEN software (Carl Zeiss AG).

Western blot analysis

Cells were washed with PBS and treated with lysis buffer (1% [w/v] SDS, 10 mM Tris-HCl, 1 mM EDTA, pH 8.0 supplemented with cOmplete Mini Protease Inhibitor and PhosSTOP phosphatase inhibitor cocktails (Roche) followed by sonication. After

measuring protein concentrations, samples were standardized to the same protein concentration. 5x sample buffer (0.35 M Tris-HCl, pH 6.8, 10%[w/v] SDS, 25% glycerol, 0.075% bromophenol blue) with 80 mM dithiothreitol was added to the samples, followed by boiling for 5 min at 95°C. Twenty μL samples were separated by SDS-polyacrylamide gel electrophoresis, transferred to polyvinylidene difluoride membranes and blocked with 5% nonfat milk in PBS-T (phosphate-buffered saline containing 0.1% Tween-20) buffer. The membranes were probed with primary antibodies overnight at 4°C and detected with horseradish peroxidase-conjugated secondary antibodies and ECL Western Blotting Detection Reagents (GE Healthcare, Chicago, IL) or ECL Prime Western Blotting Detection Reagents (GE Healthcare), followed by imaging with ImageQuant LAS 4000 mini (GE Healthcare). Quantification of band intensities was performed with ImageJ (NIH, Bethesda, MD).

Cell migration assay

Cells were plated uniformly into 35 mm Collagen type I-coated glass based dish (Iwaki, Tokyo, Japan) and grown to 95% confluence. A scratch was made using a 200-uL pipette tip, floating cells were washed off with phosphate-buffered saline (PBS), and fresh medium containing 0.5% FBS was added to suppress cell growth. The cells were incubated for the indicated periods of time, followed by exposure to UVC radiation. After a duration of 3 h following exposure, the cells were fixed with paraformaldehyde (4%, 15 min), followed by immunofluorescent (IF) staining.

For the assessment of cell migration, 24 wounds in 4 dishes were photographed at zero time and after 16 h. The wound areas were analyzed using the ImageJ software. The wound closure was calculated using the formula that wound closure =

(A0-A16)/A0×100%, where A0 represents the original wound area at 0 hr, and A16 represents the wound area at 16 hr.

EdU proliferation assay

To quantify cell proliferation in live cells, the EdU proliferation kit (iFuor 488) (Abcam, ab219801) was used according to the manufacturer's instruction. EdU solution (10 μM) was incubated with cells for 3 h at 37°C in 5% CO_2 humidified air. Cells were then fixed with 4% formaldehyde for 15 min and permeabilized. EdU detection was performed on a flow cytometer with the pretreatment as described in the provided instruction.

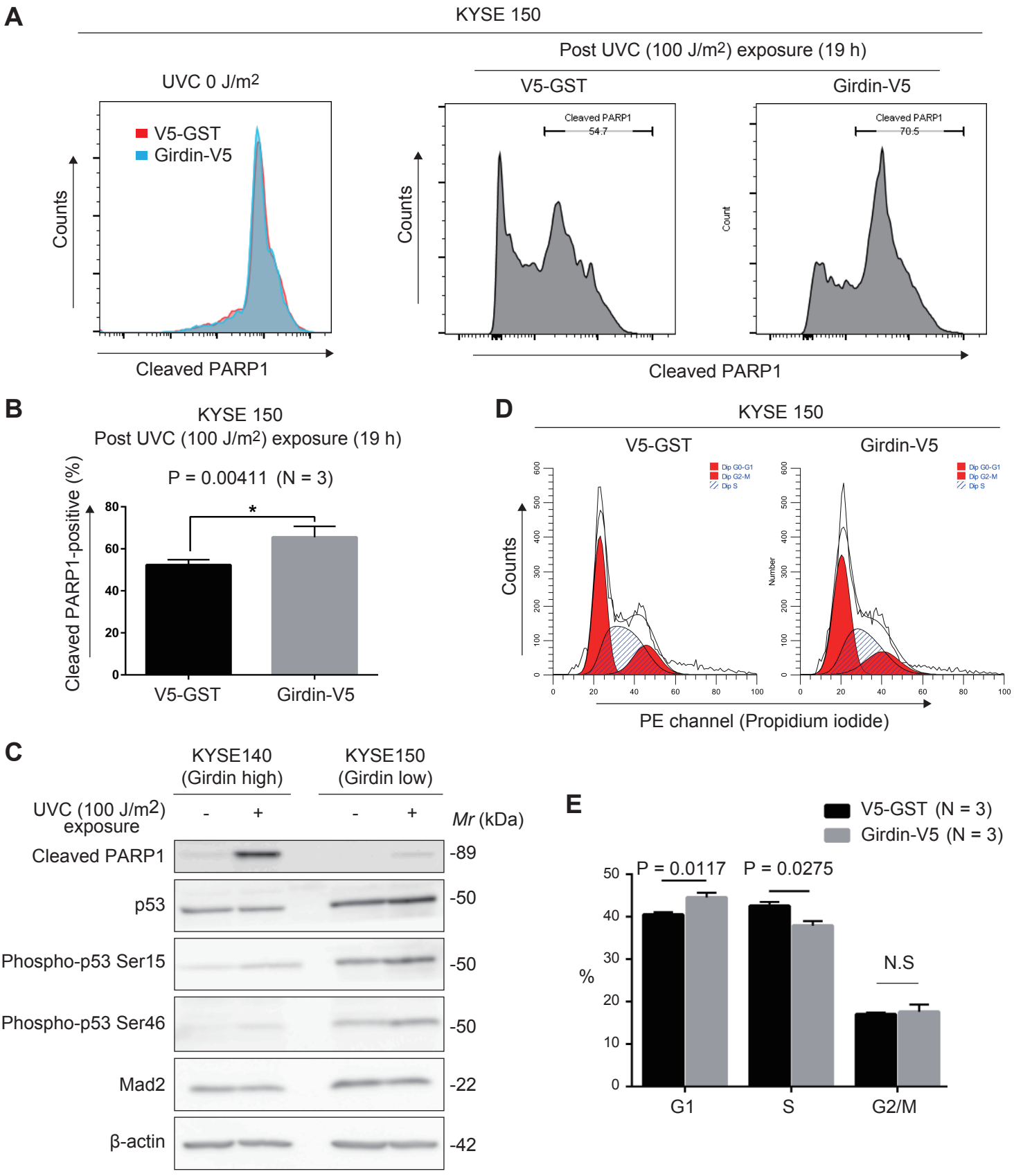

Figure S1. Effects of Girdin OE on UVC-mediated apoptosis and cell cycle progression in esophageal cancer cells
(A, B) Non-synchronized KYSE150 cells transiently transfected with V5-GST (control) or Girdin tagged with the V5 epitope (Girdin-V5) were exposed to UVC irradiation, followed by flow cytometric analysis to detect cleaved PARP1-positive cells. Representative flow histograms are shown in **(A)**, and the percentages of cleaved PARP1-positive cells are quantified in **(B)**. Results are expressed as the means ± SD of 3 independent experiments. GST, glutathione S-transferase.
(C) KYSE140 and KYSE150 cells were exposed to UVC irradiation and incubated for 19 h, followed by Western blot analysis with the indicated antibodies.
(D, E) Non-synchronized KYSE150 cells transfected with V5-GST and Girdin-V5 were stained for PI (propidium iodide), followed by flow cytometric analysis. The crosshatched areas and those filled with orange and red represent S, G1, and G2/M phases, respectively, which were determined through curve fitting with the ModFitLT software. The percentages of cells in each phase were quantified in **(E)**. Results are expressed as the means ± SD of 3 independent experiments.

Fig. S1

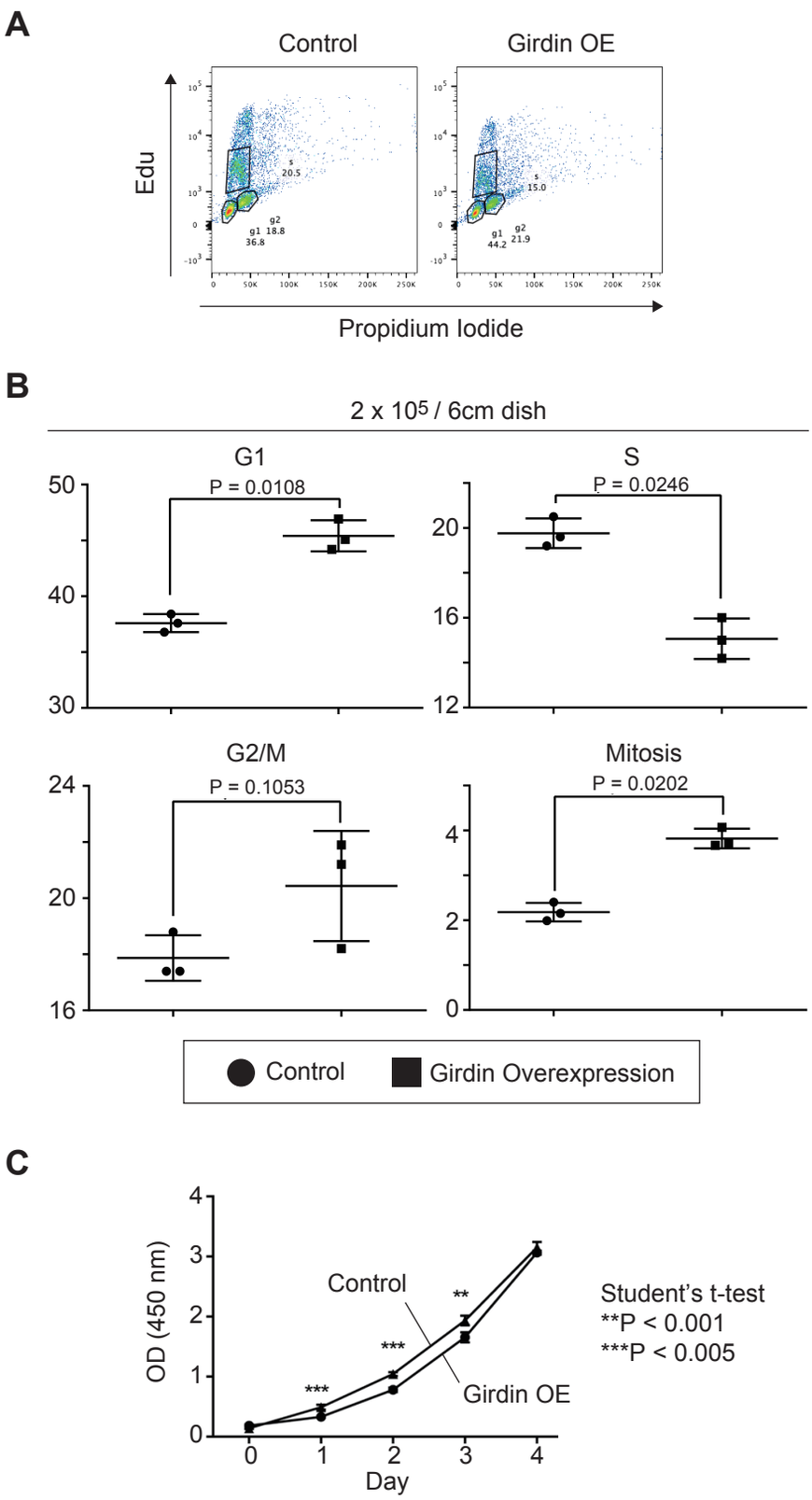

Figure S2. Girdin OE HeLa cells exhibit dysregulated cell cycle progression with prolonged G1 and M phases
(A, B) Non-synchronized control and Girdin OE HeLa cells were incubated with EdU (10 μM) for 3 h, followed by flow cytometric analysis. Representative flow histograms depicting the indicated fractions are shown in **(A)**, and the percentages of cells in the indicated cell cycle phases are quantified in **(B)**. Results are expressed as the means ± SD of 3 independent experiments.
(C) Control and Girdin OE cells were seeded on petri dishes (10^4 cells per dish), and the proliferation of the cells was quantified by the WST-1 assay.

Fig. S2

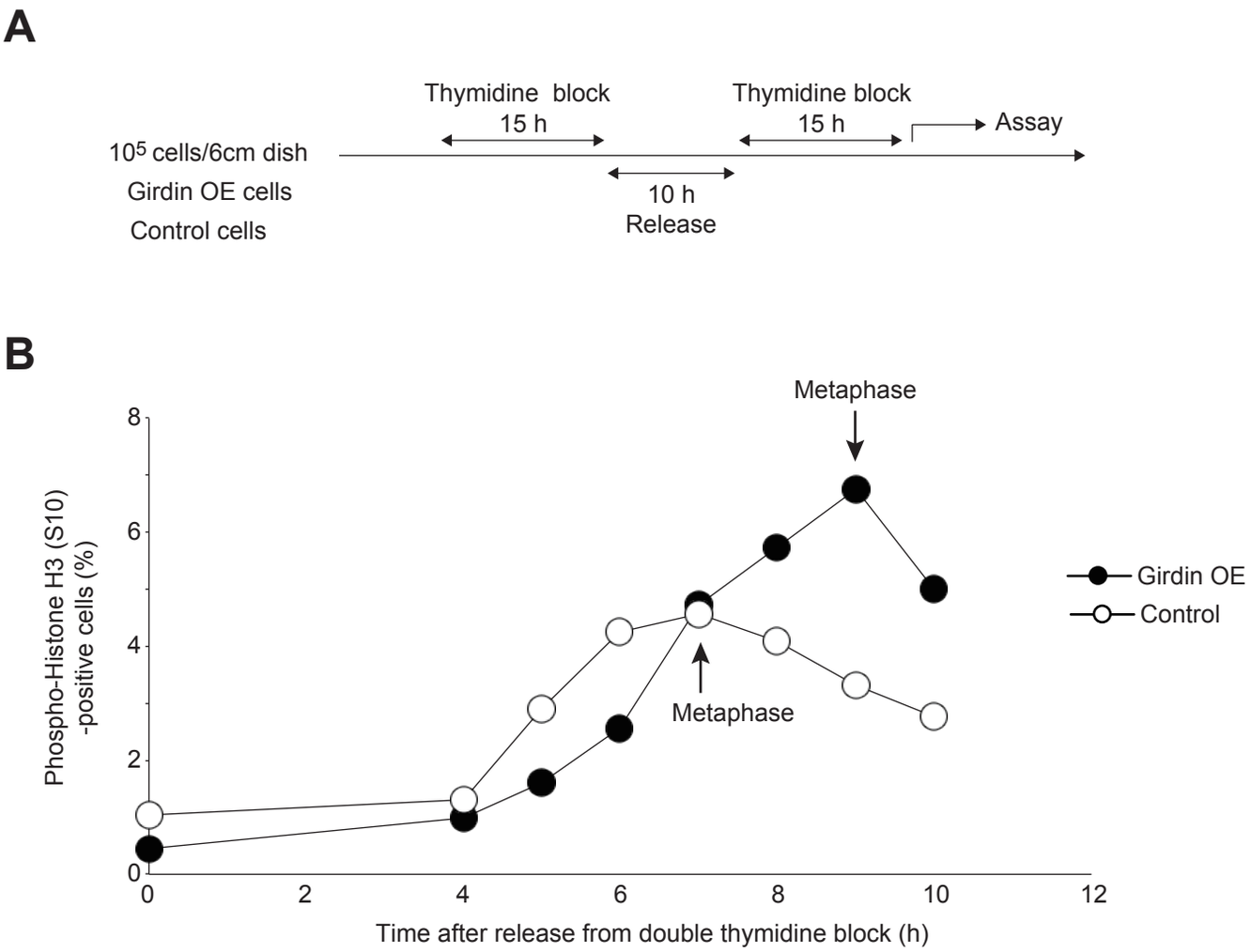

Figure S3. M phase progression analysis in control and Girdin OE HeLa cells synchronized by double thymidine block

(A) HeLa cells were incubated with thymidine (2 mM) for 15 h and released for 10 h, followed by treatment with thymidine (2 mM) for additional 15 h.

(B) Temporal changes in the percentages of phospho-Histone H3 (S10)-positive control (open circles) and Girdin OE (closed circles) cells after releasing from thymidine block were examined by flow cytometric analysis. The peaks in the number of phospho-Histone H3 (S10)-positive cells are indicated by arrows.

Fig. S3

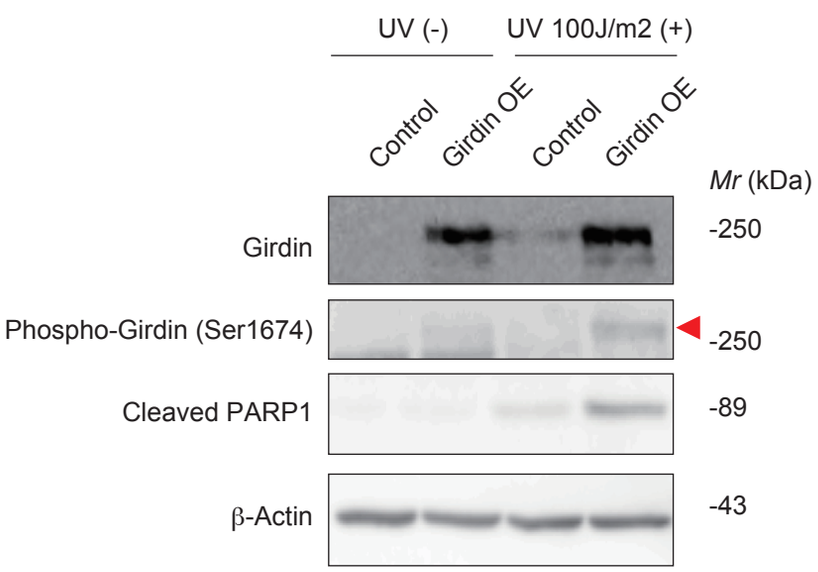

Figure S4. Cdk5-mediated Girdin phosphorylation in control and Girdin OE HeLa cells after UVC irradiation
Control and Girdin OE HeLa cells were exposed to UVC irradiation and incubated for 3 h, followed by Western blot analysis with the indicated antibodies. A red arrowhead denotes a band that represents Girdin phosphorylated by Cdk5 at Ser1674.

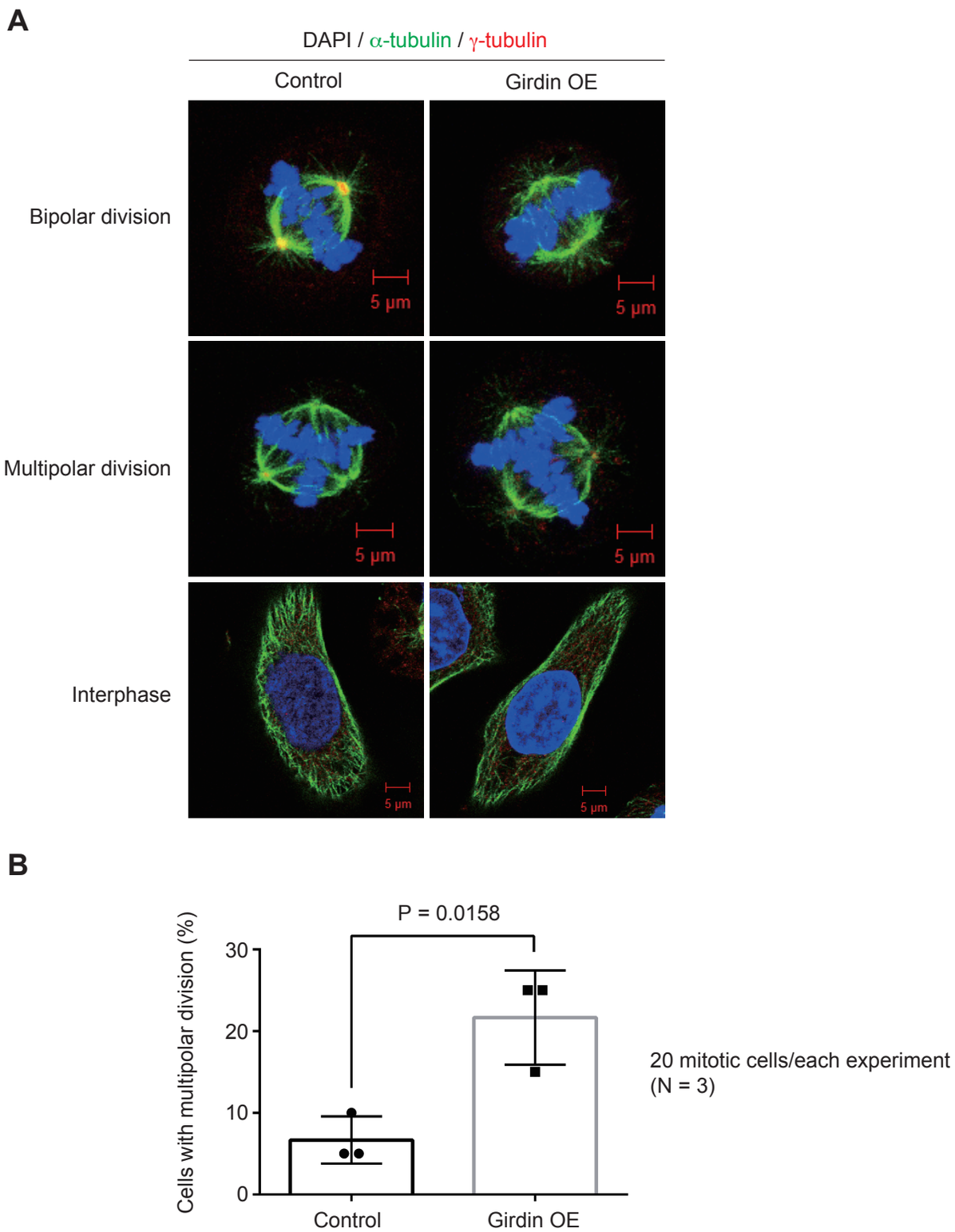

Figure S5. Organization of microtubules and mitotic spindles in control and Girdin OE HeLa cells
(A) Control (left) and Girdin OE (right) HeLa cells were fixed with -20ºC methanol and stained for microtubules by tubulin antibodies. Chromosome DNAs were visualized by DAPI staining. Representative images for bipolar and multipolar division in metaphase or early anaphase are shown. Scale bars: 5 μm.
(B) Number of cells with multipolar division in control and Girdin OE cells were counted and quantified. Twenty mitotic cells were examined in each experiment, and the results from 3 independent experiments are shown.

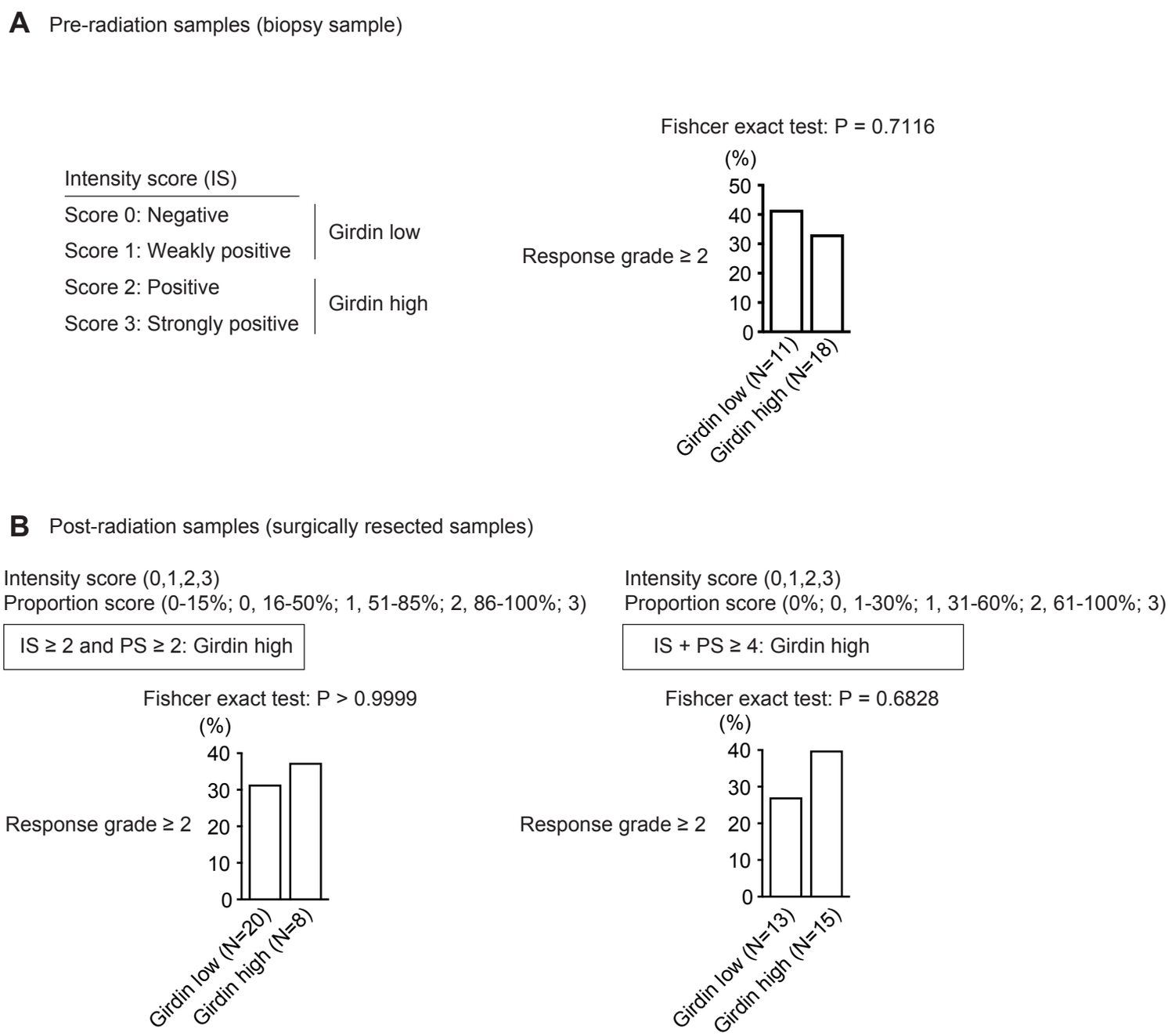

Figure S6. No significant correlation between Girdin expression and histological response to radiotherapy in esophageal cancer patients
(A) Girdin expression in pre-radiation biopsy samples taken from 29 cases of esophageal cancer was empirically evaluated by a scoring system, and the patients were classified into Girdin low and high groups (left panel). The percentage of cases with histological response greater than grade 2 in each group was plotted on the graph shown in the right panel.
(B) Girdin expression in post-radiation samples of 28 esophageal cancer cases was evaluated by two scoring systems, and the patients were classified into Girdin low and high groups (left and right panels). The percentage of cases with histological response greater than grade 2 in each group is plotted on the graphs.

Fig. S6